FINAL REPORT

on

AN INVESTIGATION OF FLAWS ON THE INSIDE SURFACE OF A TYPE 304 STAINLESS STEEL SCHEDULE 80 PIPE

to

POWER AUTHORITY OF THE STATE OF NEW YORK
JAMES A. FITZPATRICK NUCLEAR POWER PLANT

July 30, 1982

by

R. D. Buchheit

BATTELLE
Columbus Laboratories
505 King Avenue
Columbus, Ohio 43201

Battelle
Columbus Laboratories
505 King Avenue
Columbus, Ohio 43201
Telephone (614) 424-6424
Telex 24-5454

July 30, 1982

Mr. A. V. Sorentino
Power Authority of the
State of New York
10 Columbus Circle
New York, New York 10019

Dear Mr. Sorentino:

Enclosed are 10 copies of our final report entitled "An Investigation of Flaws on the Inside Surface of a Type 304 Stainless Steel Schedule 80 Pipe". This report describes the details of our investigation, conducted as was proposed in our letter of March 26, 1982, and the results we obtained. The report is a sequel to our report entitled "A Metallographic Investigation of a Type 304 Stainless Steel Schedule 80 Pipe", dated March 25, 1982.

Briefly, the results of the investigation led to the basic conclusions that (1) the flaws on the inside surface of the subject pipe were induced during pipe-fabrication processing and (2) that surface flaws located within the region of the sensitized heat-affected zone of the circumferential weld probably served as the initiation sites of intergranular stress-corrosion cracking IGSCC). Surface flaws that were located away from the weld beyond the heat-affected zone apparently did not induce IGSCC or any other mode of failure.

The interest in this investigation was very high among all of our personnel involved in the work, and we enjoyed performing the various tasks described in the report. If you have any questions concerning our work or the results obtained, please feel free to contact me.

Very truly yours,

R. D. Buchheit

R. D. Buchheit
Physical Metallurgy Section

RDB:rw

Enc. (10)

TABLE OF CONTENTS

	Page
INTRODUCTION	1
SUMMARY	2
EXPERIMENTAL PROCEDURE	3
EXAMINATIONS AND RESULTS	6
Chemical Analyses	6
Crack-Profile Determinations	6
Flaw No. 1 in Figure 1	6
Flaw No. 4 in Figure 1	14
Examinations of Other Surface Flaws	19
Energy-Dispersive X-ray Analyses	24
Corrosion Products in Flaw No. 1	24
Corrosion Products in Flaw No. 2	33
Corrosion Products in Flaw No. 5	35
Electrochemical-Polarization-Reactivation (EPR) Tests	41
DISCUSSION	45
CONCLUSIONS	46

LIST OF TABLES

TABLE 1.	Results of Emission-Spectrographic Analyses of the Type 304 Stainless Steel Pipe and the Stainless Steel Weld Metal of the Circumferential Weld	7
TABLE 2.	Crack-Depth and Crack-Length Data for the IGSCC Associated with Flaw No. 1	10
TABLE 3.	Crack-Depth and Crack-Length Data for the IGSCC Associated with Flaw No. 4	16

LIST OF TABLES
(Continued)

Page

TABLE 4. Results of Semiquantitative[a] Electron-Microprobe Analyses of Corrosion Products by Energy-Dispersive-X-ray Analytical Techniques in Specimen 1-S-S of Flaw No. 1 25

TABLE 5. Results of Semiquantitative[a] Electron-Microprobe Analyses of Corrosion Products by Energy-Dispersive-X-ray Analytical Techniques in Specimens 2-N-N and 2-R-R of Flaw No. 2 34

TABLE 6. Results of Semiquantitative[a] Electron-Microprobe Analyses of Corrosion Products by Energy-Dispersive X-ray Analytical Techniques in Specimen 5-U-U- of Flaw No. 5 41

LIST OF FIGURES

FIGURE 1. Inside Surface of the Schedule 80 Stainless Steel Pipe Showing Surface Flaws, the Locations of Metallographic and EPR Test Specimens, and the Circumferential Weld . . 4

FIGURE 2. Profile of Intergranular Stress-Corrosion Crack at Flaw No. 1 9

FIGURE 3. The IGSCC Associated With Flaw No. 1 at Several Locations Along the Length of the Crack. 11

FIGURE 4. Flaw No. 1 Near the End of the IGSCC Farthest From the Weld. 12

FIGURE 5. The Flow Pattern of Metal Around Flaw No. 1 at the 0.72-Inch Location in Figure 2 13

FIGURE 6. Profile of Intergranular Stress-Corrosion Crack at Flaw No. 4 15

FIGURE 7. The IGSCC Associated With Flaw No. 4 at Several Locations Along the Length of the Crack. 17

FIGURE 8. The Flow Pattern of Metal Around Surface Flaw No. 2 Observed in Specimen 2-P-P 20

FIGURE 9. The Flow Pattern of Metal Around Surface Flaw No. 2 in Specimen 2-N-N 21

LIST OF FIGURES
(Continued)

		Page
FIGURE 10.	The Flow Pattern of Metal Around Surface Flaw No. 2 in Specimen 2-R-R	22
FIGURE 11.	The Flow Pattern of Metal Around Surface Flaw No. 5 in Specimen 5-U-U	23
FIGURE 12.	Energy-Dispersive X-ray Spectrum Obtained From an Analysis of the Type 304 Stainless Steel Matrix in Specimen 1-S-S of Flaw No. 1 (Area 1 in Table 4)	27
FIGURE 13.	Cross Section of Flaw No. 1 in Section 1-S-S	28
FIGURE 14.	Energy-Dispersive X-ray Spectrum Obtained From an Analysis of Corrosion Products in Flaw No. 1 Observed in Specimen 1-S-S (Area 3 in Table 4)	29
FIGURE 15.	Corrosion Products in the IGSCC Near the Inside Surface of the Pipe	30
FIGURE 16.	Energy-Dispersive X-ray Spectrum Obtained From an Analysis of Corrosion Products in the Crack (Area 4 in Table 4)	31
FIGURE 17.	Energy-Dispersive X-ray Spectrum Obtained From an Analysis of Corrosion Products in a Branch Crack (Area in Table 4)	32
FIGURE 18.	Energy-Dispersive X-ray Spectrum Obtained From an Area Scan of Corrosion Products in Flaw No. 2 Specimen 2-N-N (Area 1 in Table 5)	36
FIGURE 19.	Corrosion Products in Flaw No. 2 That Were Subjected to Electron-Microprobe Analyses	37
FIGURE 20.	EPR Curves for Sample EPR-2 From the Weld Heat-Affected Zone	43
FIGURE 21.	EPR Curves for Samples EPR-1 ID and EPR-1 OD, AISI Stainless Steel Pipe Remote From the Region of the Weld	44

AN INVESTIGATION OF FLAWS ON THE INSIDE SURFACE OF A TYPE 304 STAINLESS STEEL SCHEDULE 80 PIPE

by

R. D. Buchheit

INTRODUCTION

The subject investigation is a sequel to a previous investigation conducted by Battelle's Columbus Laboratories (BCL) of a linear defect that was detected on the inside surface of a pipe section using nondestructive ultrasonic-inspection techniques. The pipe section was a section of a 12-inch-diameter Type 304 stainless steel Schedule 80 seamless pipe that was a part of the core-spray system for a boiling-water reactor at the James A. Fitzpatrick Nuclear Power Plant of the Power Authority of the State of New York (PASNY). Descriptions of the details and the results of the previous investigation are contained in the BCL report entitled " A Metallographic Investigation of a Type 304 Stainess Steel Schedule 80 Pipe", dated March 25, 1982. The summary of that report is repeated below.

> "Macroscopic examination of the inside surface of a 12-inch-diameter Type 304 stainess steel seamless pipe revealed the presence of numerous linear defects in addition to one that was detected by PASNY using nondestructive ultrasonic-inspection techniques. A cross section through one of the linear defects that was located close to a weld was examined metallographically. The results of the examination indicated that the linear defect was most likely a fabrication-induced surface flaw that resembled a lap or seam. The surface flaw apparently acted as a stress raiser and, in the presence of a corrosive environment (the water contained in the pipe) and under the influence of hoop stresses induced by the internal pressure and possibly residual stresses in the hoop direction, it led to the

initiation and propagation of an intergranular stress-corrosion crack through a sensitized region in the weld heat-affected zone."

The objectives of the subject investigation of the same section of pipe that was examined previously were (1) to examine and characterize other selected surface flaws and determine the presence or absence of cracks associated with those flaws, (2) to determine the profile of the cracks found to be present, (3) to obtain qualitative chemical analyses of corrosion products found in surface flaws and in cracks, (4) to evaluate the susceptibility of the subject pipe material to intergranular stress-corrosion cracking (IGSCC), and (5) to determine the chemical compositions of the subject pipe material and the circumferential weld metal contained in the pipe section.

The procedures used to meet the objectives of the investigation conducted by BCL and the results obtained are described in this report.

SUMMARY

Cross sections of several surface flaws were examined metallographically with the light microscope, and the susceptibility of the Type 304 stainless steel pipe to intergranular stress-corrosion cracking (IGSCC) was evaluated by electrochemical-polarization-reactivation (EPR) tests.

The cross sections through surface flaws located in the weld heat-affected zone exhibited IGSCC that had initiated and propagated from the base of those flaws. Profiles of two IGSCC's were determined from measurements of the crack depth versus crack length obtained on metallographic serial sections prepared at various intervals along the lengths of the cracks.

The cross sections through surface flaws located in regions remote from the weld heat-affected zone did not reveal the presence of IGSCC or other modes of failure associated with the surface flaws. All surface flaws exhibited characteristics of laps or seams. The appearance of the flaws and the flow patterns of metal around them indicated that the flaws were fabrication-induced during the process of forming the seamless pipe.

EPR tests indicated that the weld heat-affected zone that was sensitized was susceptible to IGSCC, whereas parent metal remote from the weld heat-affected zone was not. However, there appeared to be no IGSCC in the weld heat-affected zone in the absence of a surface flaw in that region. Hence, the surface flaws, probably acting as stress raisers, were apparently a major factor that contributed to the initiation and propagation of the IGSCC's.

Electron-microprobe analyses of corrosion products in the surface flaws and in the IGSCC's using energy-dispersive X-ray analytical techniques did not identify the corrodent(s). The corrodent was most likely the water in the core-spray system that may have contained low concentrations of oxygen and chloride that were not detected by the electron-microprobe analyses.

The chemical compositons of both the weld metal and the pipe material were found to conform to the AISI specificiations for Type 304 stainless steel.

EXPERIMENTAL PROCEDURE

The photograph in Figure 1 shows the portion of the inside surface of the Schedule 80 pipe and the surface flaws that were observed during the previous investigation. (This photograph appeared as Figure 3 in the BCL report of the previous investigation and, also, as Figure 1 in BCL's proposal for this present investigation.) The surface flaws that were selected for further studies are identified in Figure 1 by the arrows numbered 1, 2, 4 and 5. Those flaws, as numbered, conform to the manner in which those flaws were identified in BCL's proposal for this investigation. The feature identified by the arrow that was numbered 3 in that proposal is actually a part of Flaw No. 2 and is now identified as Section R-R of Flaw No. 2 in Figure 1.

Metallographic cross sections through each of the four selected flaws and perpendicular to them, as shown in Figure 1, were prepared for microscopic examinations. The resulting metallographic specimens were identified as Specimen 1-S-S for Section S-S of Flaw No. 1, Specimen 1-T-T for

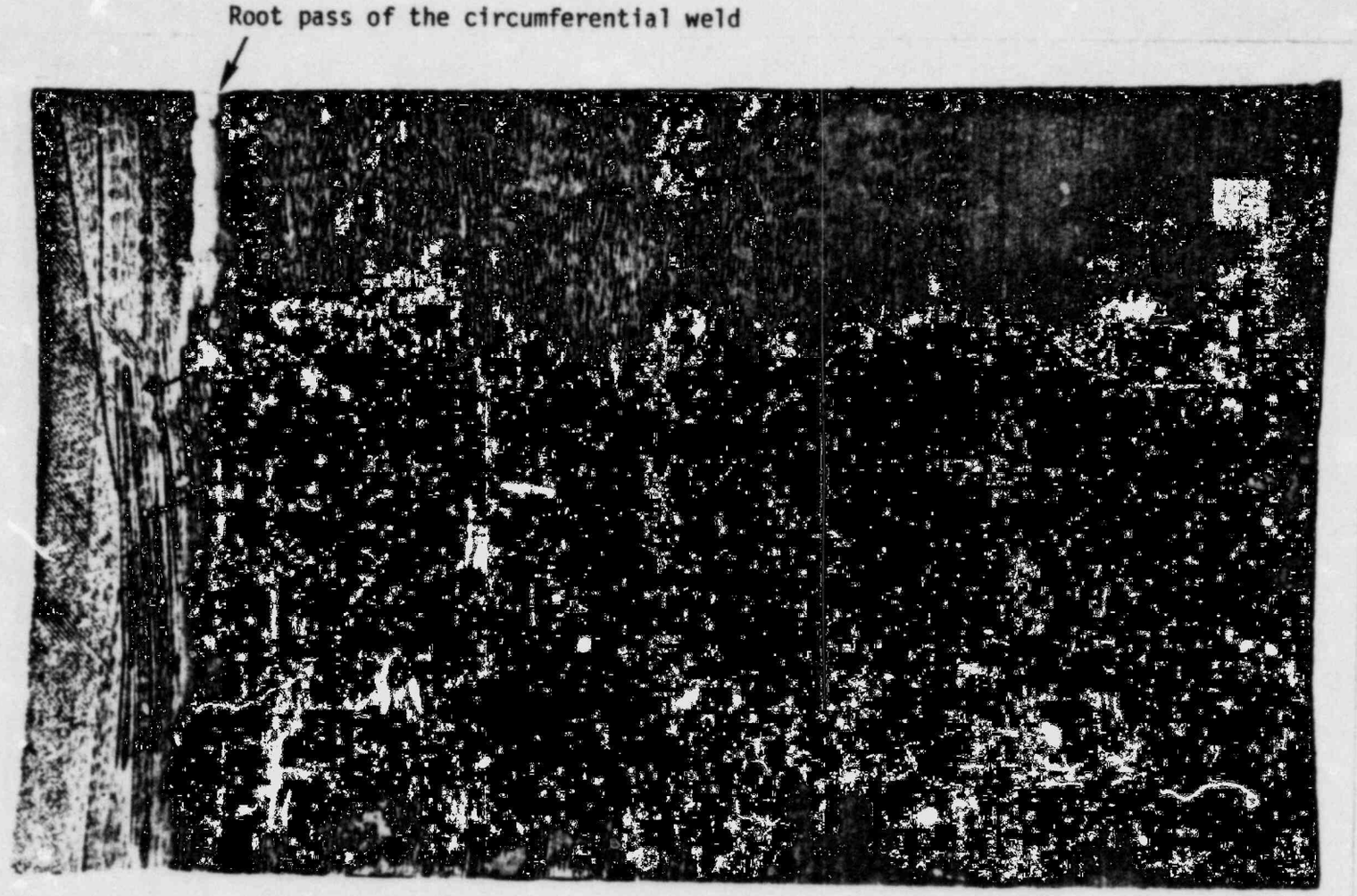

~1X

7K253

FIGURE 1. INSIDE SURFACE OF THE SCHEDULE 80 STAINLESS STEEL PIPE SHOWING SURFACE FLAWS, THE LOCATIONS OF METALLOGRAPHIC AND EPR TEST SPECIMENS, AND THE CIRCUMFERENTIAL WELD

Section T-T of Flaw No. 1, Specimen 2-P-P for Section P-P of Flaw No. 2, et cetera, for the remainder of the cross sections indicated in Figure 1.

The cross sections that revealed cracks, namely, Specimens 1-S-S, 1-T-T, 4-K-K, and 4-L-L, were successively ground, polished, and examined at measured incremental depths below each successive polished surface to establish the profiles of the cracks along the lengths of the flaws. The incremental depth measurements served as intervals of distance along the length of the crack. At each successive plane of polish, the depth of the crack below the inside surface of the pipe and the maximum width of the crack were measured using a digital measuring microscope. Maximum crack widths always were found at or near the surface unless the crack did not penetrate the surface. The crack-depth and crack-length measurements were plotted to reveal the profile of the crack in two dimensions.

Chemical analyses of corrosion products observed in surface flaws and in cracks were obtained using energy-dispersive-X-ray (EDAX) analytical techniques in conjunction with a scanning electron microscope. Both area-scan and spot analyses were performed. The EDAX results were reported as semiquantitative analyses. The semiquantitative analysis is a standardless quantitative analysis of the X-ray-energy-spectrum data that includes a full ZAF (atomic number, absorption, and fluorescence factors) matrix-correction calculation. The relative concentrations of the elements detected are normalized to obtain a sum of 100 percent. The energy-dispersive system does not detect the lighter elements, i.e., elements of atomic number lower than 11 (sodium). Thus, for example, the concentration of oxygen that is frequently a major element in corrosion products is not included in the results of EDAX analyses.

The locations of samples used to evaluate the susceptibility of the pipe material to IGSCC are identified in Figure 1 by EPR-1 ID, EPR-1 OD, and EPR-2. The evaluation was accomplished by performing electrochemical-polarization-reactivation (EPR) tests of the inside and outside pipe surfaces some distance from the weld and of a region of the weld heat-affected zone. A through-wall piece of the pipe approximately 1/2 inch square was sectioned in half at the midwall to provide Sample EPR-1 ID for the inside pipe surface and Sample EPR-1 OD for the outside pipe surface. Those surfaces were

ground slightly and polished to provide suitable flat surfaces for the EPR tests. A polished cross section of the weld heat-affected zone was obtained to provide Sample EPR-2. Since experience has shown that the presence of weld metal in the test sample interferes with the results of the EPR test, all of the weld metal in Sample EPR-2 was ground away.

Quantitative chemical analyses of the pipe material and the weld metal were obtained using emission-spectographic analytical techniques. The analysis of the pipe material was determined on the surface of a through-wall section of the pipe that was obtained from a location adjacent to the location of the EPR-1 ID and EOR-1 OD samples. The analysis of the weld metal was determined on the surface of a through-wall section of the pipe along the center line of the weld; that section of the weld was obtained from a location that was adjacent to the location of the EPR-2 sample.

EXAMINATIONS AND RESULTS

Chemical Analyses

The chemical compositions of the Type 304 stainless steel Schedule 80 pipe and the circumferential weld metal that joined the straight-pipe section to an elbow section are presented in Table 1. The specified composition of AISI Type 304 stainless steel is included in Table 1 for comparison. The chemical compositions of both the pipe and the weld metal were found to conform to the AISI specifications for Type 304 stainless steel.

Crack-Profile Determinations

Flaw No. 1 in Figure 1

The metallographic examination of Specimen 1-S-S (see Figure 1) during the previous investigation of the Schedule 80 pipe revealed the presence of IGSCC extending from the bottom of Flaw No. 1 at the inside pipe surface toward the outside surface through about 77 percent of the wall thickness. In the present investigation, the profile of that crack along

TABLE 1. RESULTS OF EMISSION-SPECTROGRAPHIC ANALYSES OF THE TYPE 304 STAINLESS STEEL PIPE AND THE STAINLESS STEEL WELD METAL OF THE CIRCUMFERENTIAL WELD

Element	Content, weight percent		
	Pipe	AISI Type 304 Specifications	Weld Metal
Carbon	0.045	0.08 max	0.032
Manganese	1.73	2.0 max	1.42
Phosphorus	0.021	0.045 max	0.014
Sulfur	0.016	0.030 max	0.007
Silicon	0.65	1.0 max	0.63
Nickel	10.3	8-10.5	9.6
Chromium	18.3	18-20	19.1
Molybdenum	0.18		0.10
Vanadium	0.05		0.05
Aluminum	0.007		0.042
Copper	0.10		0.065
Tin	0.008		0.006
Columbium	0.008		0.011
Zirconium	0.005		0.006
Titanium	0.004		0.006
Boron	0.0005		0.0007
Cobalt	0.11		0.10
Tungsten	0.00		0.00
Iron	68.73		68.78

its length was obtained from serial sections of Specimen 1-S-S and Specimen 1-T-T; the profile is revealed in Figure 2 by a plot of the depths of the crack below the inside pipe surface at various intervals of distance along the length of the crack. Zero distance in Figure 2 corresponds to the location (termed a reference plane) where no crack was observed beyond the end of the flaw next to the weld metal; in this case, the reference plane was entirely within the weld metal The abscissa in Figure 2 extends away from the weld through its heat-affected zone and in a direction along the length of the flaw. The crack-depth and crack-length data that are plotted in Figure 2 are given in Table 2.

The cross-hatched region in Figure 2 represents the extent of the IGSCC surface. Included in Figure 2 are the approximate locations of the inside and outside pipe surfaces and portions of the weld line with respect to the crack. Note that IGSCC penetrated weld metal where crack propagation eventually arrested. However, crack propagation extended a short distance beyond the final pass of weld metal on the outside pipe surface and, in fact, reached the outside surface in one small region. It is interesting to note here that no leakage of the core-spray pipe system was reported.

Figure 3 shows the appearance of the IGSCC at a few locations along its length. Figure 3a exhibits the crack at the 0.060-inch position. At that location the crack was subsurface and entirely within weld metal. At the 0.290-inch position, Figure 3b, the crack extended through approximately 77 percent of the pipe wall. Figure 3c exhibits the portion of the crack near the outside surface of the pipe at the 0.702-inch position (at much higher magnification); essentially the entire crack in the through-wall direction is shown.

The appearance of the surface flaw at the 0.70-inch position is revealed in Figure 4. The flaw exhibited two surface imperfections that were approximately 0.1 inch apart; those two inperfections are shown in Figures 4a and 4b respectively. A little IGSCC was still evident at the flaw shown in Figure 4b.

The flow pattern of the metal that developed around the flaw during the fabrication of the pipe was revealed by etching metallographically polished specimens, as is shown in Figure 5 at a magnification of 50X. At

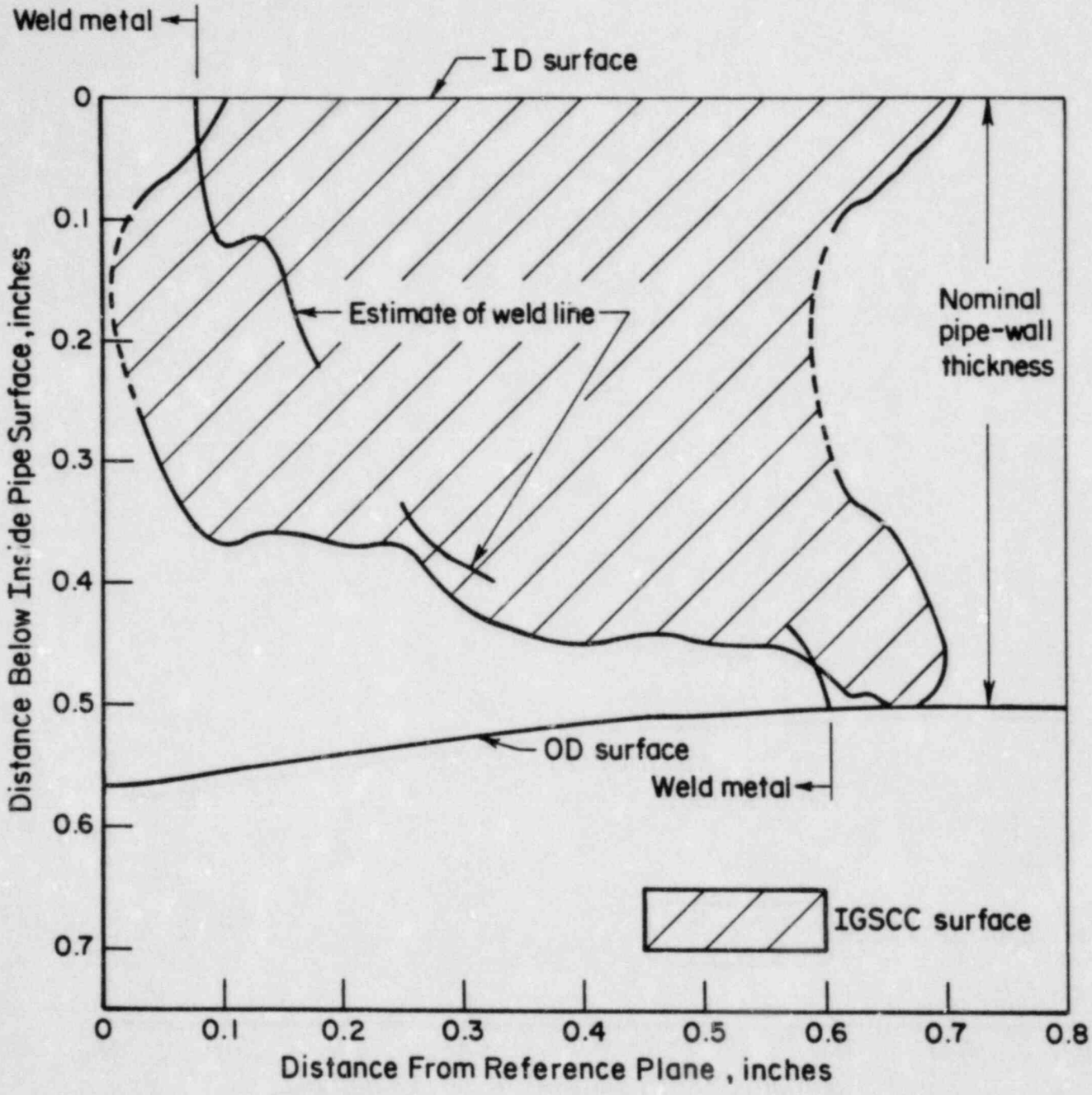

FIGURE 2. PROFILE OF INTERGRANULAR STRESS-CORROSION CRACK AT FLAW NO. 1

TABLE 2. CRACK-DEPTH AND CRACK-LENGTH DATA FOR THE IGSCC ASSOCIATED WITH FLAW NO. 1

Specimen of Flaw No. 1	Distance from Reference Plane,(a) inches	Depth of Crack Below Inside Pipe Surface, inches	Maximum Width of Crack, mils
1-S-S	0	No crack	-
	0.030	0.092 to 0.255	0.4
	0.060	0.059 to 0.328	0.7
	0.100	0.008 to 0.373	1.0
(Surface Flaw No. 1 begins)	?		
	0.130	0.357	1.0
	0.170	0.364	1.4
	0.210	0.366	1.4
	0.250	0.366	1.7
	0.290	0.410	2.0
1-T-T	0.322	0.429	2.0
	0.362	0.443	3.0
	0.412	0.448	1.0
	0.462	0.443	2.0
	0.512	0.447	2.0
	0.562	0.449	2.0
(Weld Metal at OD ends)	?		
	0.612	0.108 and 0.305 to 0.482	0.8 and 0.6
	0.622	0.087 and 0.326 to 0.487	0.5 and 0.4
	0.637	0.083 and 0.337 to 0.492	0.8 and 0.4
	0.652	0.069 and 0.349 to 0.497	0.9 and 0.3
	0.677	0.043 and 0.391 to 0.496	0.7 and 0.3
	0.702	0.019 and 0.452 to 0.470	0.4 and 0.1
(Flaw No. 1 ends)	?		
	0.717	No crack	-

(a) The distance from a reference plane of polish just beyond the end of the crack that was in the weld.

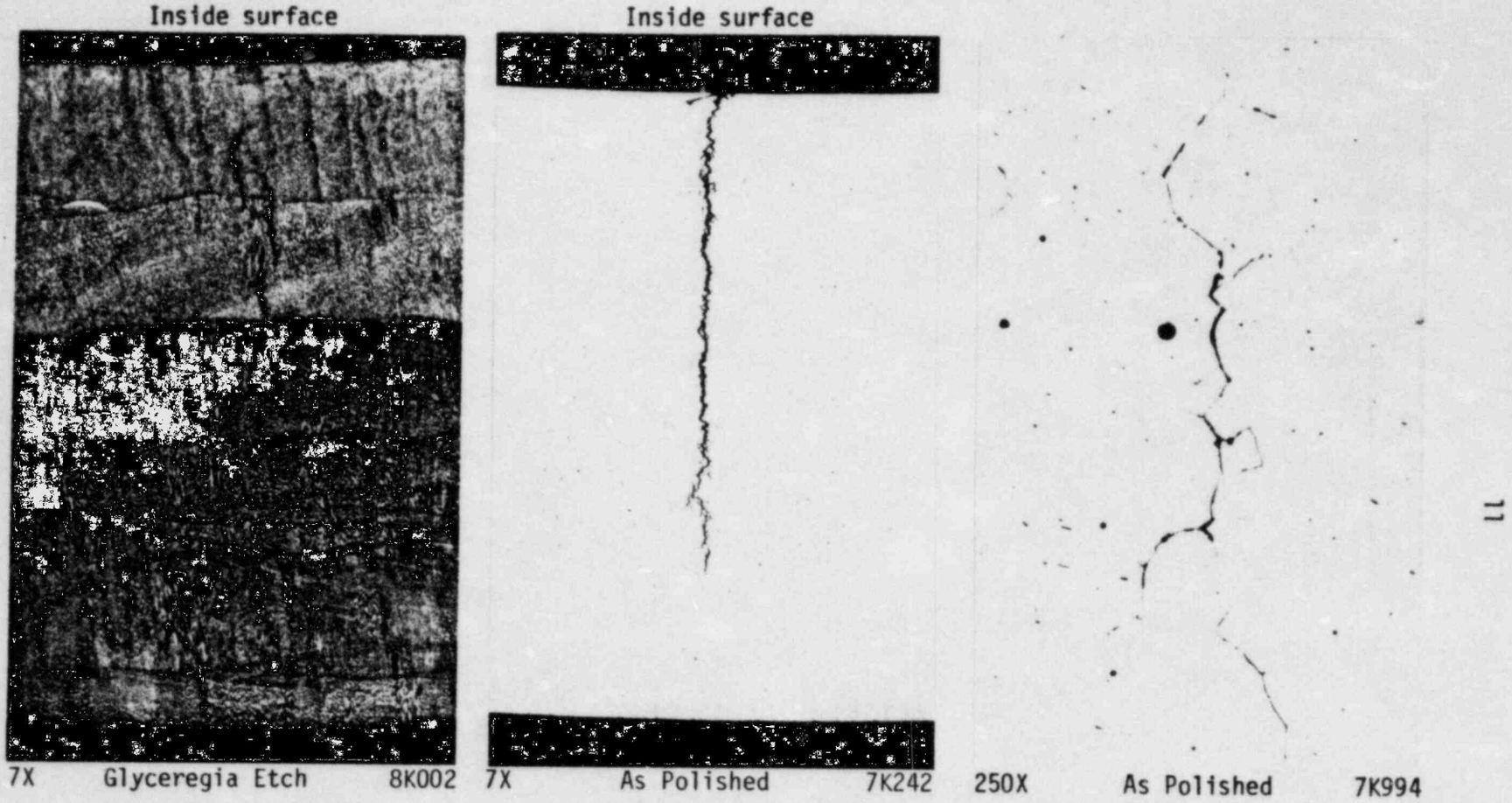

7X Glyceregia Etch 8K002

a. IGSCC at the 0.060-Inch Position

7X As Polished 7K242

b. IGSCC at the 0.290-Inch Position

250X As Polished 7K994

c. IGSCC Near the Outside Surface of the Pipe at the 0.70-Inch Position

FIGURE 3. THE IGSCC ASSOCIATED WITH FLAW NO. 1 AT SEVERAL LOCATIONS ALONG THE LENGTH OF THE CRACK

100X 7K993

a. Surface Imperfection Located About 0.1 Inch from the Imperfection Shown in (b) Below

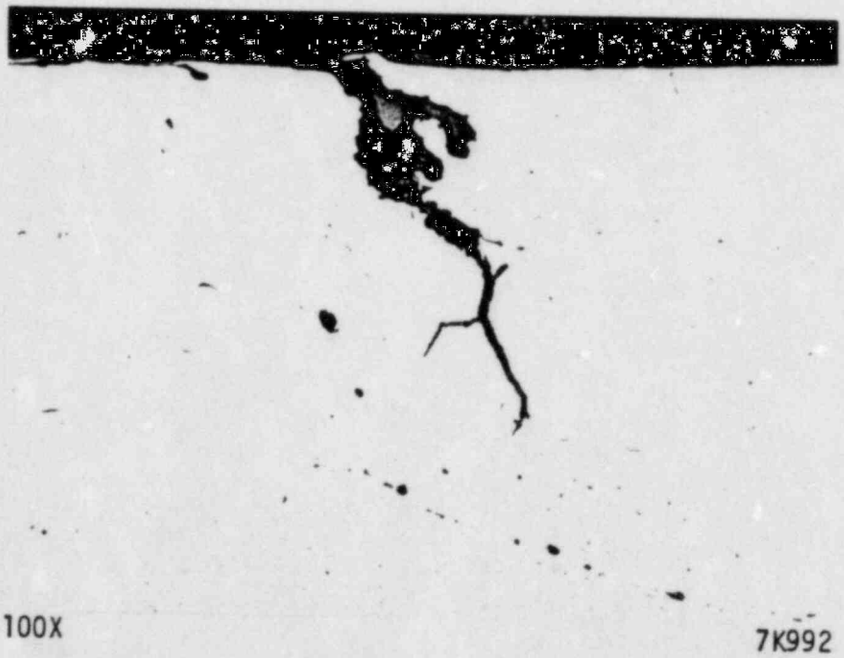

100X 7K992

b. Surface Imperfection and Some IGSCC at the 0.70-Inch Position

FIGURE 4. FLAW NO. 1 NEAR THE END OF THE IGSCC FARTHEST FROM THE WELD

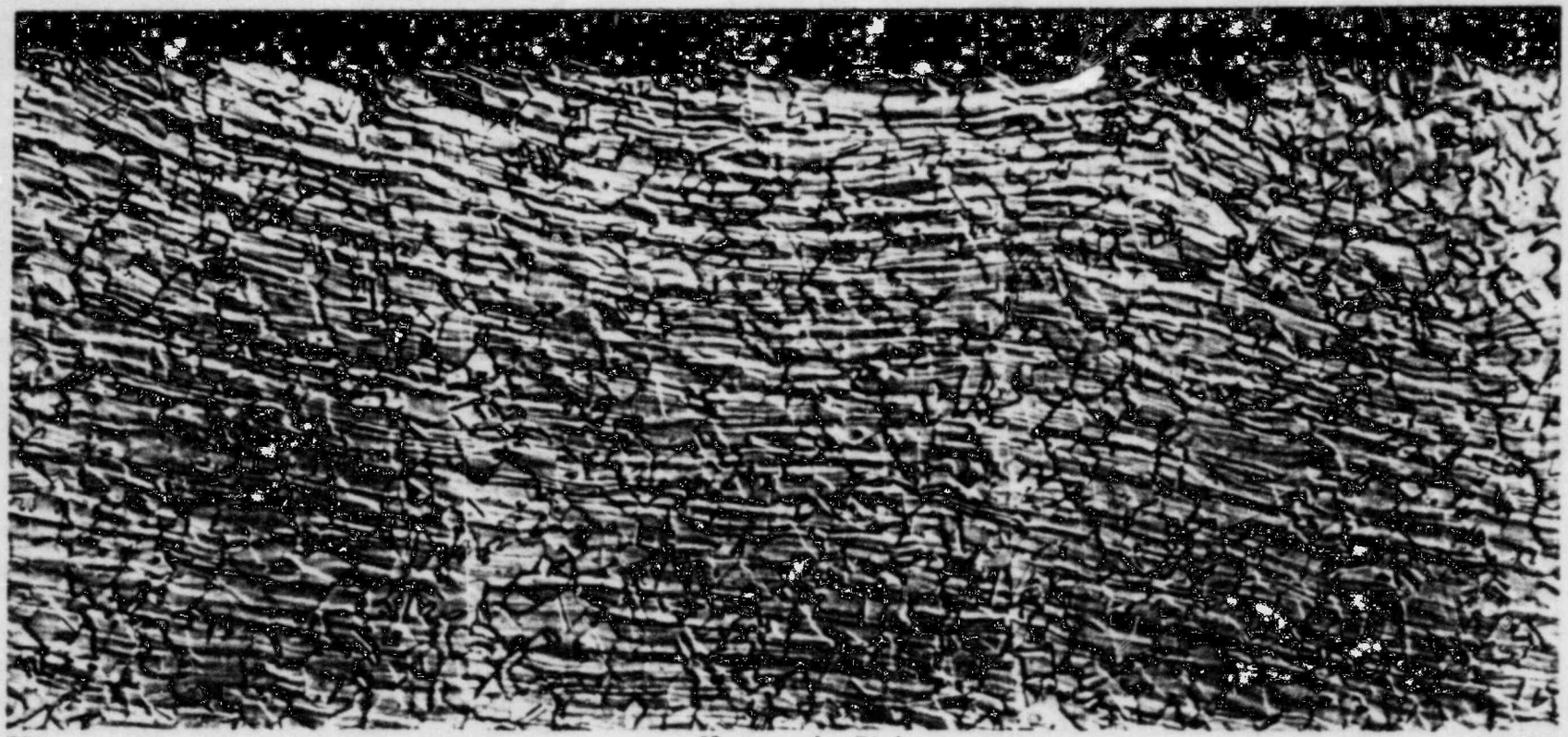

50X Glyceregia Etch 8K018

FIGURE 5. THE FLOW PATTERN OF METAL AROUND FLAW NO. 1 AT THE 0.72-INCH LOCATION IN FIGURE 2

The photomicrograph was taken using Nomarski interference-contrast microscopy to enhance the metal-flow pattern.

that magnification, the two surface imperfections shown in Figure 4a and 4b are evident. The cross section of the flaw in Figure 5 is located at approximately the 0.72-inch position in Figure 2; that cross section is about 0.02 inch beyond the cross section shown in Figure 4. In Figure 5, the surface imperfection shown in Figure 4a is observed to be slightly larger, and the surface imperfection shown in Figure 4b is observed to be slightly smaller with little or no evidence of IGSCC,

Flaw No. 4 in Figure 1

Flaw No. 4, like Flaw No. 1, was located in close proximity to the weld in the region of the weld heat-affected zone. At that location, the propagation of IGSCC from the flaw was suspected and was observed in metallographic cross sections of the flaw. The profile of the crack was obtained from serial sections of Specimen 4-K-K and Specimen 4-L-L. When Specimen 4-K-K was prepared metallographically, it was anticipated that no crack would be present in the initial section, because the section was obtained beyond the end of the flaw that was visible on the surface of the pipe. However, a crack was present; therefore Specimen 4-L-L was prepared in order to determine the extent of the crack in a direction away from the weld. The profile of the IGSCC crack at Flaw No. 4 is revealed in Figure 6 in the same manner as was the crack-profile presented in Figure 2. The data for crack depth and crack length that are plotted in Figure 6 are given in Table 3.

The cross-hatched region in Figure 6 represents the extent of the IGSCC surface. Included in Figure 6 are the approximate locations of the inside and outside pipe surfaces and a portion of the weld line, with respect to the crack. Although the crack-surface area was smaller, the general outline of that area was similar to that of the IGSCC at Flaw No. 1 (compare Figures 2 and 6). Also, arrest of the crack propagation in the through-wall direction again apparently occurred in weld metal.

Figure 7 shows the appearance of the IGSCC at a few locations along its length. Figure 7a exhibits the crack at the 0.10-inch position. At that location, the crack was subsurface and was entirely within weld metal except for a very small portion near middepth. At the 0.125-inch position (Figure 7b), the crack was slightly beneath the inside surface of the pipe and had begun to

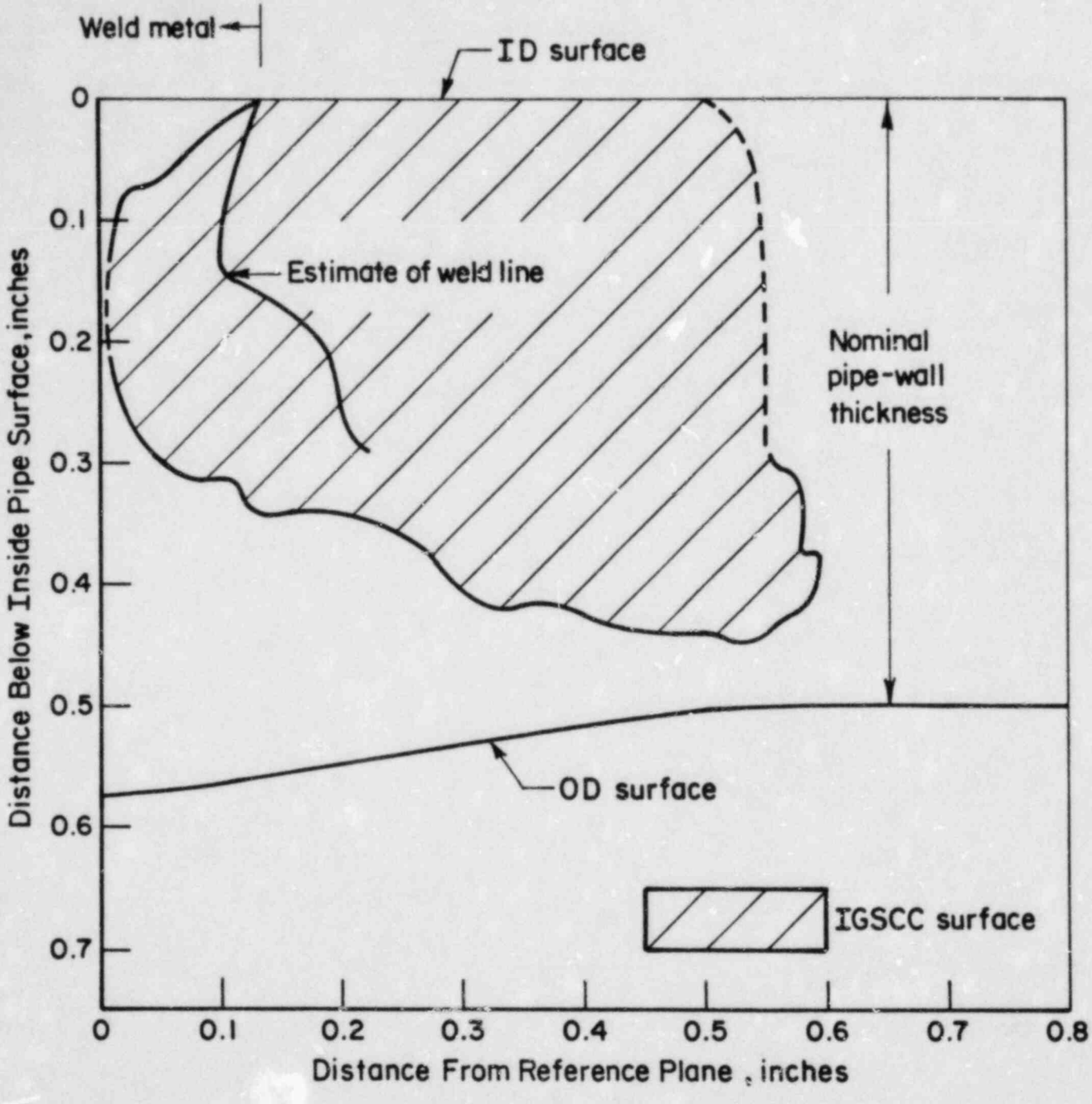

FIGURE 6. PROFILE OF INTERGRANULAR STRESS-CORROSION CRACK AT FLAW NO. 4

TABLE 3. CRACK-DEPTH AND CRACK-LENGTH DATA FOR THE IGSCC ASSOCIATED WITH FLAW NO. 4

Specimen of Flaw No. 4	Distance from Reference Plane,(a) inches	Depth of Crack Below Inside Pipe Surface, inches	Maximum Width of Crack, mils
4-K-K	0	No crack	-
	0.010	0.133 to 0.213	0.2
	0.022	0.081 to 0.256	0.5
	0.047	0.069 to 0.296	1.0
	0.097	0.023 to 0.315	1.0
	0.112	0.014 to 0.315	1.0
	0.127	0.004 to 0.341	1.0
	0.142	0.345	1.2
	0.161	0.340	1.2
	0.187	0.338	1.8
	0.212	0.346	1.3
	0.262	0.367	1.6
	0.312	0.415	1.0
	0.372	0.415	1.5
	0.431	0.437	1.0
	0.491	0.441	0.6
	0.511	0.008 to 0.441	0.5
	0.517	0.012 to 0.444	0.5
4-L-L	0.554	0.295 to 0.438	0.3
	0.559	0.299 to 0.437	0.2
	0.565	0.305 to 0.431	0.15
	0.575	0.313 to 0.425	0.15
	0.585	0.373 to 0.415	0.1
	0.597	0.376 to 0.385	0.05
	0.607	No crack	-

(a) The distance from a reference plane of polish just beyond the end of the crack that was in the weld.

a. IGSCC at the 0.10-Inch Position

b. IGSCC at the 0.125-Inch Position

c. IGSCC at the 0.161 Inch Position

FIGURE 7. THE IGSCC ASSOCIATED WITH FLAW NO. 4 AT SEVERAL LOCATIONS ALONG THE LENGTH OF THE CRACK

7X As Polished 7K998

d. IGSCC at the 0.517-Inch Position

500X As Polished 7K997

e. IGSCC at the 0.597-Inch Position

FIGURE 7. (Continued)

penetrate the root pass of the weld. Figure 7c shows the crack at the 0.161-inch position.

The first plane of polish in Specimen 4-K-K revealed the IGSCC as shown in Figure 7d. As was mentioned earlier, the presence of a crack in this plane of polish was not anticipated, because Specimen 4-K-K was beyond the visible end of Flaw No. 4. Not only was the crack present, but the depth of the crack was nearly a maximum and a second, adjacent crack was observed. The second crack is evident in Figure 7d to the left of the primary crack. In this section, both the primary crack and the secondary crack began below the inside surface of the pipe. Neglecting the distance between the pipe surface and the beginning of the crack below the pipe surface, the primary crack extended in depth about 89 percent of the pipe-wall thickness. The secondary crack was not plotted in Figure 6, because its presence was observed only between the 0.49- and 0.52-inch locations and it did not extend beyond a depth below the pipe surface of about 0.12 inch. The secondary crack may have been a branch of the primary crack.

Figure 7e exhibits the IGSCC crack near the outside suface of the pipe at about the 0.60-inch position at high magnification; the entire crack in the through-wall direction is shown. No crack was observed in the next serial section beyond 0.60 inch.

Examinations of Other Surface Flaws

The examinations of cross sections of other surface flaws, namely Specimens 2-P-P, 2-N-N, 2-R-R, and 5-U-U (see Figure 1), did not reveal the presence of IGSCC nor any other mode of failure induced by the surface flaws. All of the surface flaws examined exhibited characteristics similar to those generally observed for seams or laps in billet surfaces. Examples of those characteristics are shown in Figures 8 through 11. The three cross sections of Flaw No. 2 are presented in Figures 8 through 10. In Specimen 2-P-P in Figure 8, the depth of Flaw No. 2 was observed to be relatively shallow. The slight depression in the surface of the pipe, indicated by the arrow in Figure 8, and the curved flow pattern of metal below that depression suggest that a thin, sliver of surface metal may have been present at that location

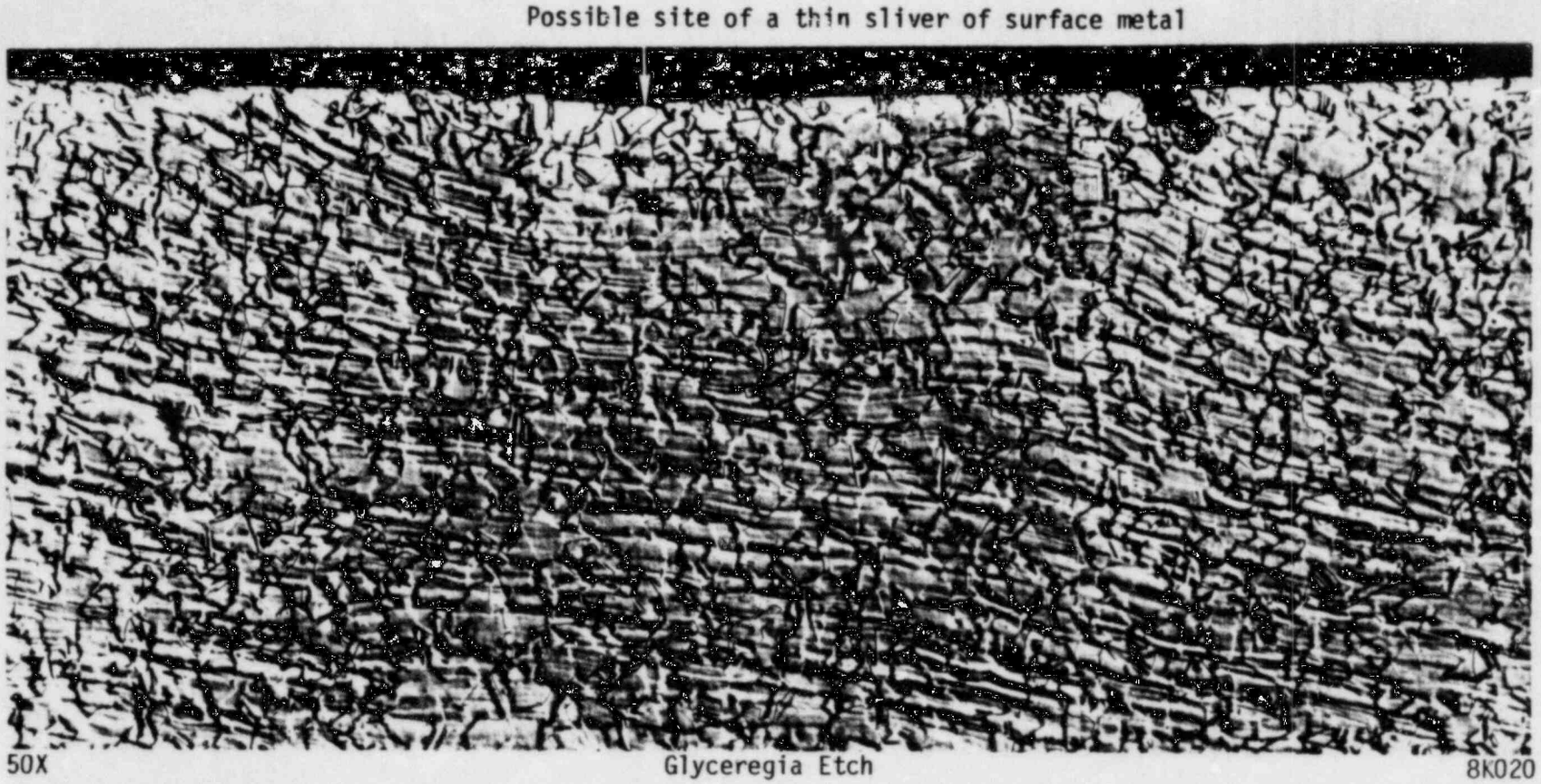

FIGURE 8. THE FLOW PATTERN OF METAL AROUND SURFACE FLAW NO. 2 OBSERVED IN SPECIMEN 2-P-P

The photomicrograph was taken using Nomarski interference-contrast microscopy to enhance the metal-flow pattern.

FIGURE 9. THE FLOW PATTERN OF METAL AROUND SURFACE FLAW NO. 2 IN SPECIMEN 2-N-N

The photomicrograph was taken using Normarski inteference-contrast microscopy to enhance the metal-flow pattern.

50X Glyceregia Etch 8K021

FIGURE 10. THE FLOW PATTERN OF METAL AROUND SURFACE FLAW NO. 2 IN SPECIMEN 2-R-R

The photomicrograph was taken using Nomarksi interference-contrast microscopy to enhance the metal-flow pattern.

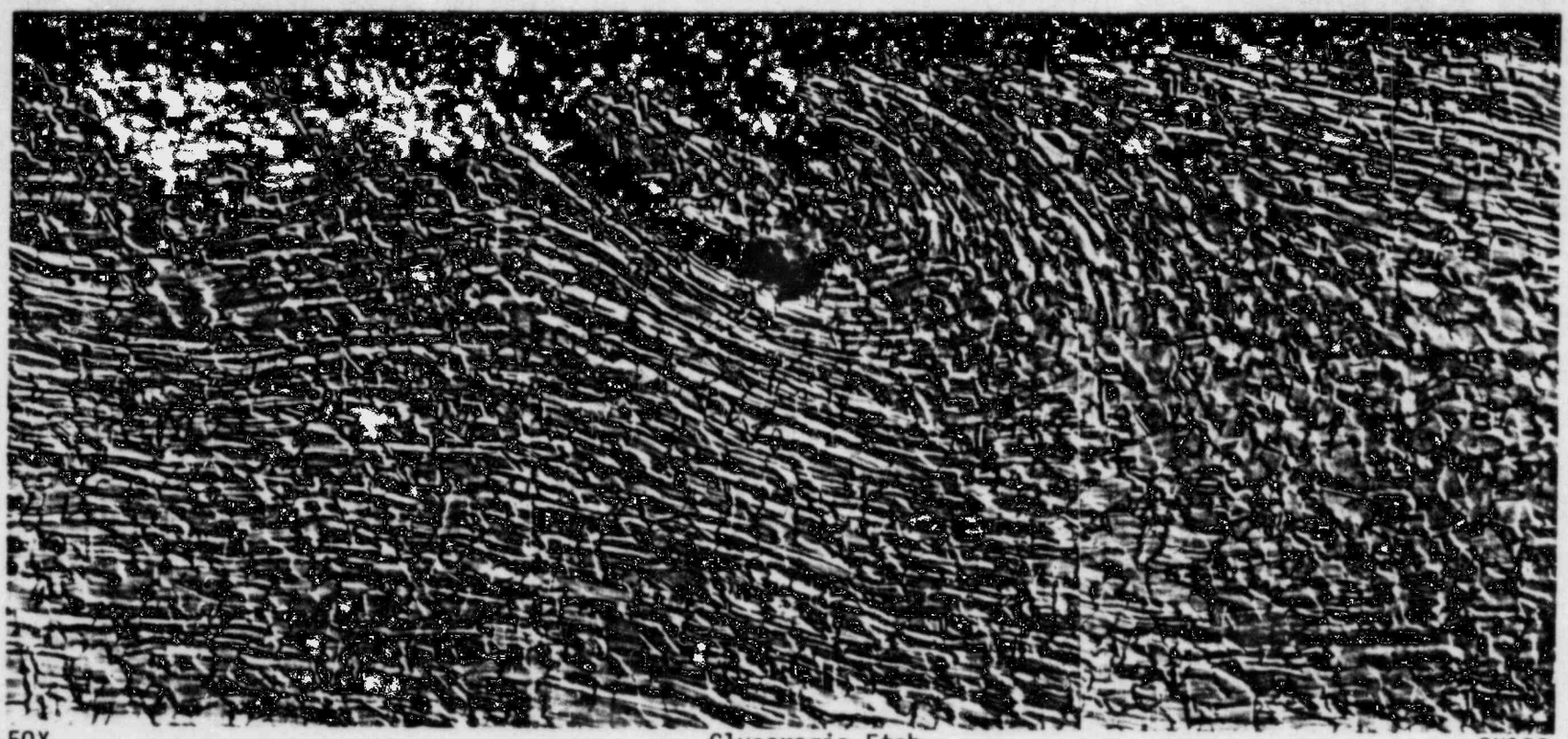

FIGURE 11. THE FLOW PATTERN OF METAL AROUND SURFACE FLAW NO. 5 IN SPECIMEN 5-U-U

The photomicrograph was taken using Nomarski interference-contrast microscopy to enhance the metal-flow pattern.

at some earlier time. Specimen 2-N-N was taken at approximately the mid-length of Flaw No. 2. In that section, shown in Figure 9, the flaw appears very much like a surface fold, or lap. The depth of the flaw was about 0.035 inch. Specimen 2-R-R was taken across a thin sliver of surface metal that had been lifted, but not removed, from the surface; the appearance of the sliver can be seen in Figure 10. Part of the sliver was detached from the surface of the pipe at the location of Specimen 2-R-R.

Specimen 5-U-U across Flaw No. 5 is shown in Figure 11. The characteristics of Flaw No. 5 were similar to those of Flaw No. 2 (and Flaw No. 1 that was presented earlier in this report and in the report of the previous investigation). The depth of Flaw No. 5 was about 0.030 inch.

The flow patterns of metal that were revealed around the flaws indicated that the surface flaws developed during the fabrication of the seamless pipe; hence, the flaws were present in the pipe when the pipe was installed in the core-spray piping system.

Energy-Dispersive X-ray Analyses

Chemical analyses of the corrosion products observed in Flaw No. 1 and the IGSCC associated with that flaw were made in Specimen 1-S-S before the serial sections were prepared. Analyses of the corrosion products in other surface flaws were made in Specimens 2-N-N and 2-R-R of Flaw No. 2 and in Specimen 5-U-U of Flaw No. 5.

Corrosion Products in Flaw No. 1

The results of the semiquantitative energy-dispersive X-ray (EDAX) electron-microprobe analyses of corrosion products observed within Flaw No. 1 in the IGSCC asscciated with the flaw are presented in Table 4. The results of EDAX analyses of the AISI 304 stainless steel pipe and the weld metal in Specimen 1-S-S are included in Table 4 as base data for comparison with the results obtained from the analyses of the corrosion products.

TABLE 4. RESULTS OF SEMIQUANTITATIVE[a] ELECTRON-MICROPROBE ANALYSES OF CORROSION PRODUCTS BY ENERGY-DISPERSIVE-X-RAY ANALYTICAL TECHNIQUES IN SPECIMEN 1-S-S OF FLAW NO. 1

	Area Analyzed	Relative Concentration of the Elements Detected[b], percent			
		Fe	Cr	Ni	Si
1	304 SS matrix	69.6	18.9	10.4	1.0
2	304 SS weld metal	69.4	19.7	9.8	1.1
3	Corrosion products in Flaw No. 1 (see Figure 13)	56.4	36.1	6.3	1.2
4	Corrosion products in the main crack near the inside pipe surface (see Figure 15)	93.9	0.9	5.3	ND[c]
5	Corrosion products in a branch crack	69.0	24.2	5.9	0.9
6	Corrosion products in a branch crack near Area 5	47.9	44.0	6.5	1.5
7	Corrosion products in the main crack at about middepth	93.3	1.3	5.3	ND
8	Corrosion products in the main crack near the crack tip in the weld metal	92.1	2.9	5.0	ND

(a) The semiquantitative analysis is a standardless quantitative analysis of the X-ray-energy-spectra data that includes a full ZAF (atomic number, absorption, and fluorescence factors) matrix-correction calculation. The relative concentrations of the elements detected are normalized to obtain a sum of 1.0 (100 percent).

(b) Elements lighter than Atomic Number 11 (sodium) are not detected, so oxygen could not be determined.

(c) ND = not detected.

The relative concentrations of chromium and nickel in the pipe (Area 1 in Table 4) and in the weld metal (Area 2 in Table 4) agree quite well with the contents of those two elements that were obtained by emission-spectrographic analytical techniques. (Refer to Table 1 for the comparison.) The X-ray-energy spectrum for the pipe, which was nearly the same as the spectrum for the weld metal, is shown in Figure 12.

The corrosion products that were analyzed in Flaw No. 1 (Area 3 in Table 4) are identified by the arrow in Figure 13, a cross section of Flaw No. 1 observed in Specimen 1-S-S. The X-ray-energy spectrum for Area 3 is presented in Figure 14. The analysis of the chromium present in the corrosion products indicated that the chromium content was nearly twice the chromium content of the pipe. The increase in the chromium content was accompanied by decreases in the iron and nickel contents.

The region represented by Area 4 in Table 4, a region of corrosion products in the IGSCC below Flaw No. 1 near the inside surface of the pipe, is shown in Figure 15a. Those corrosion products contained a relatively low concentration of chromium, as was indicated also by the X-ray-energy spectrum of Area 4 presented in Figure 16. The X-ray distribution map of chromium presented in Figure 15b indicates the low concentration of chromium in the major portion of the corrosion products in the grain boundaries. (A region that exhibits a relatively sparse population of white dots in an X-ray-distribution map of an element indicates that the region contains a lower concentration of the element than do the regions that exhibit more dense populations of white dots.) The major decrease in the chromium content was balanced by a major increase in the iron content.

Areas 5 and 6 in Table 4 were the regions of corrosion products observed in two different, but nearby, intergranular cracks that branched out from the main intergranular crack. The chromium and iron contents appeared to differ significantly between those two areas, and the chromium content in both areas was well above that in the pipe. The X-ray-energy spectrum of Area 6 is shown in Figure 17.

The analyses of corrosion products in the main crack at about middepth below the inside pipe surface and of corrosion products near the crack tip in the weld metal both exhibited relatively low concentrations of

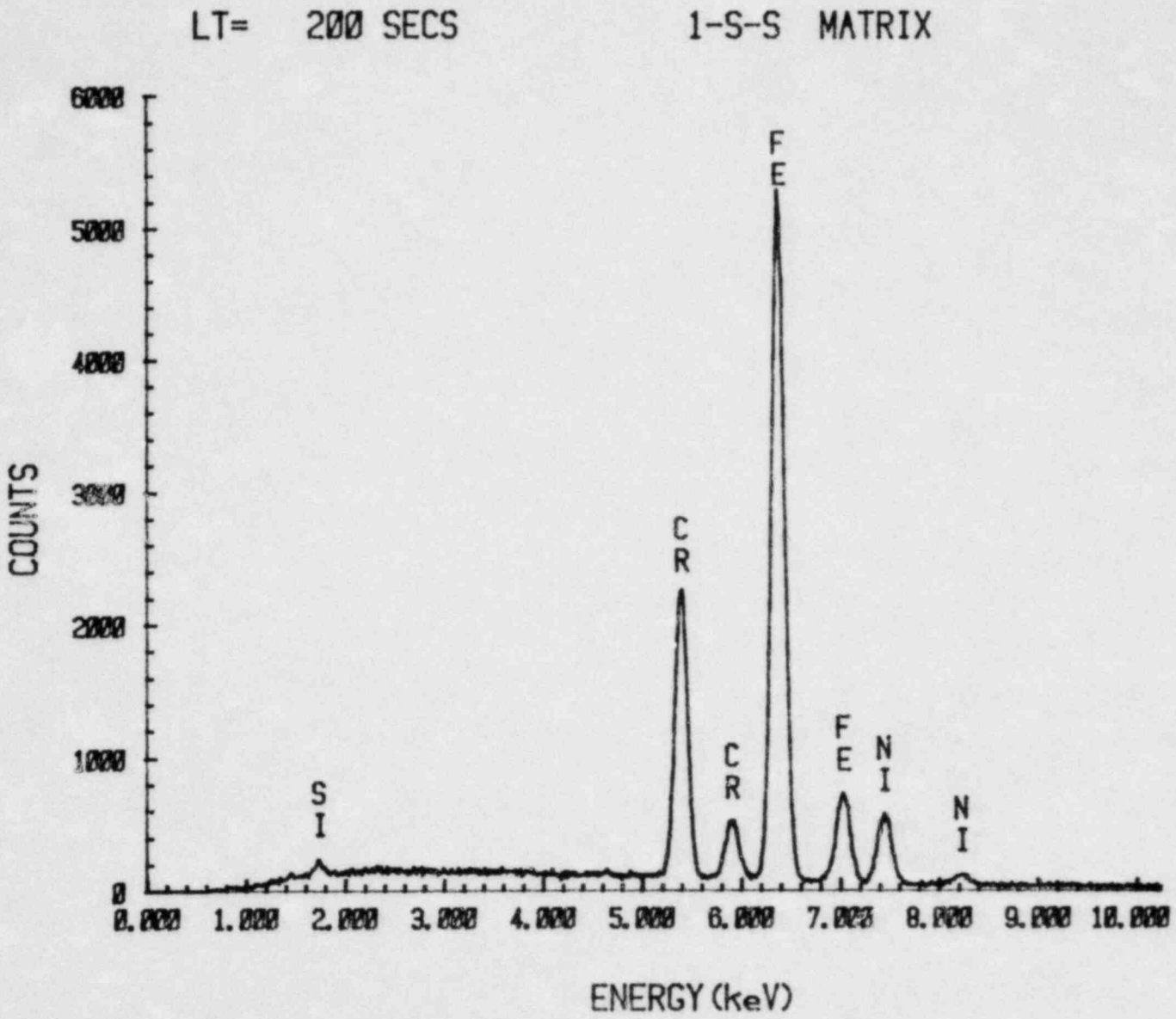

FIGURE 12. ENERGY-DISPERSIVE X-RAY SPECTRUM OBTAINED FROM AN ANALYSIS OF THE TYPE 304 STAINLESS STEEL MATRIX IN SPECIMEN 1-S-S OF FLAW NO. 1 (AREA 1 in TABLE 4)

100X As Polished 7K243

FIGURE 13. CROSS SECTION OF FLAW NO. 1 IN SECTION 1-S-S

The arrow identifies the corrosion products in Flaw No. 1 (Area 3 in Table 4) that were subjected to EDAX analyses.

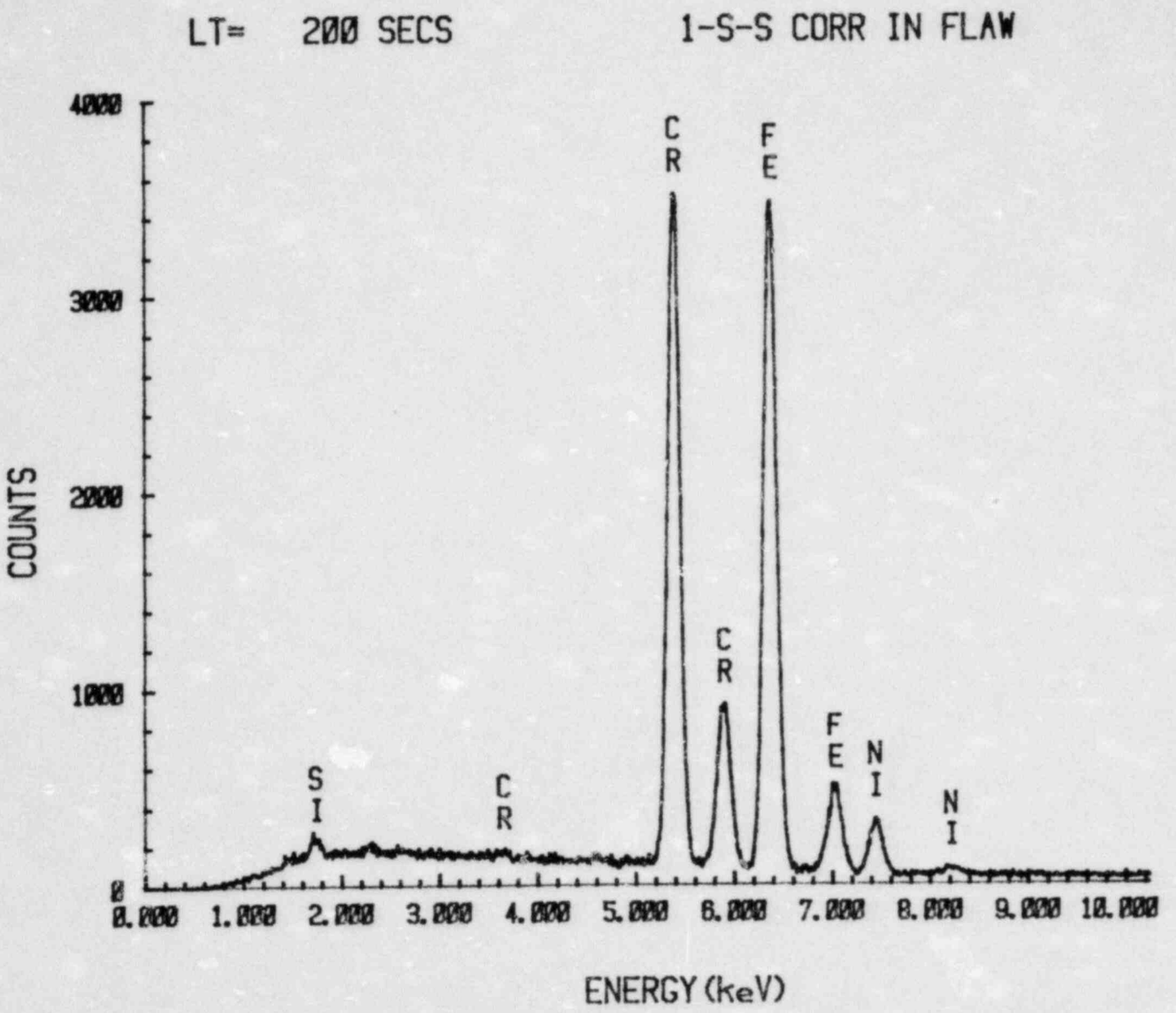

FIGURE 14. ENERGY-DISPERSIVE X-RAY SPECTRUM OBTAINED FROM AN ANALYSIS OF CORROSION PRODUCTS IN FLAW NO. 1 OBSERVED IN SPECIMEN 1-S-S (AREA 3 in TABLE 4)

1000X 34692

a. Region of the IGSCC Identified As Area 4 in Table 4 (SEM Micrograph)

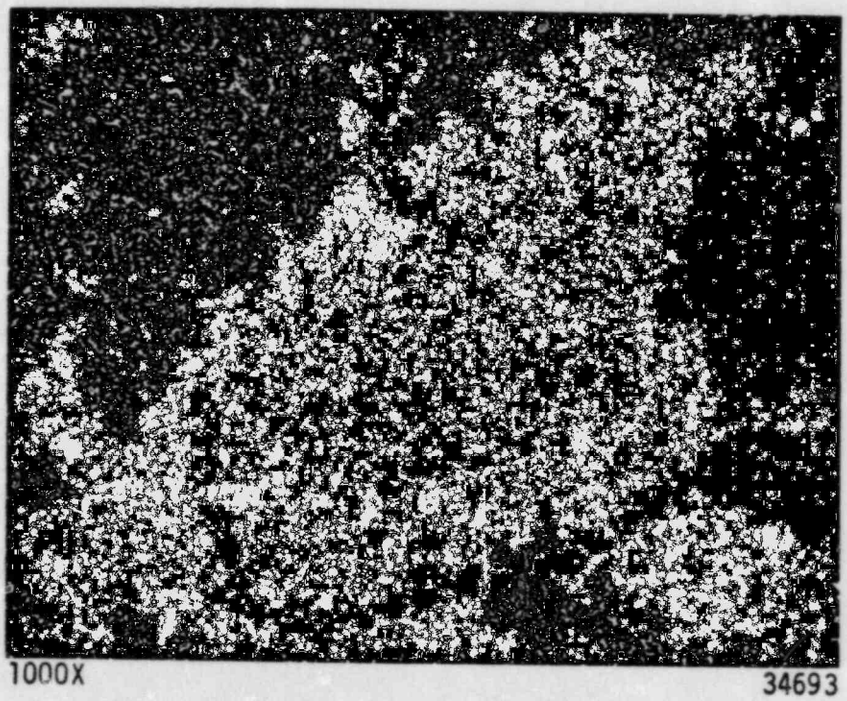

1000X 34693

b. X-ray-Distribution Map of Cr in the Region Shown in (a) Above

FIGURE 15. CORROSION PRODUCTS IN THE IGSCC NEAR THE INSIDE SURFACE OF THE PIPE

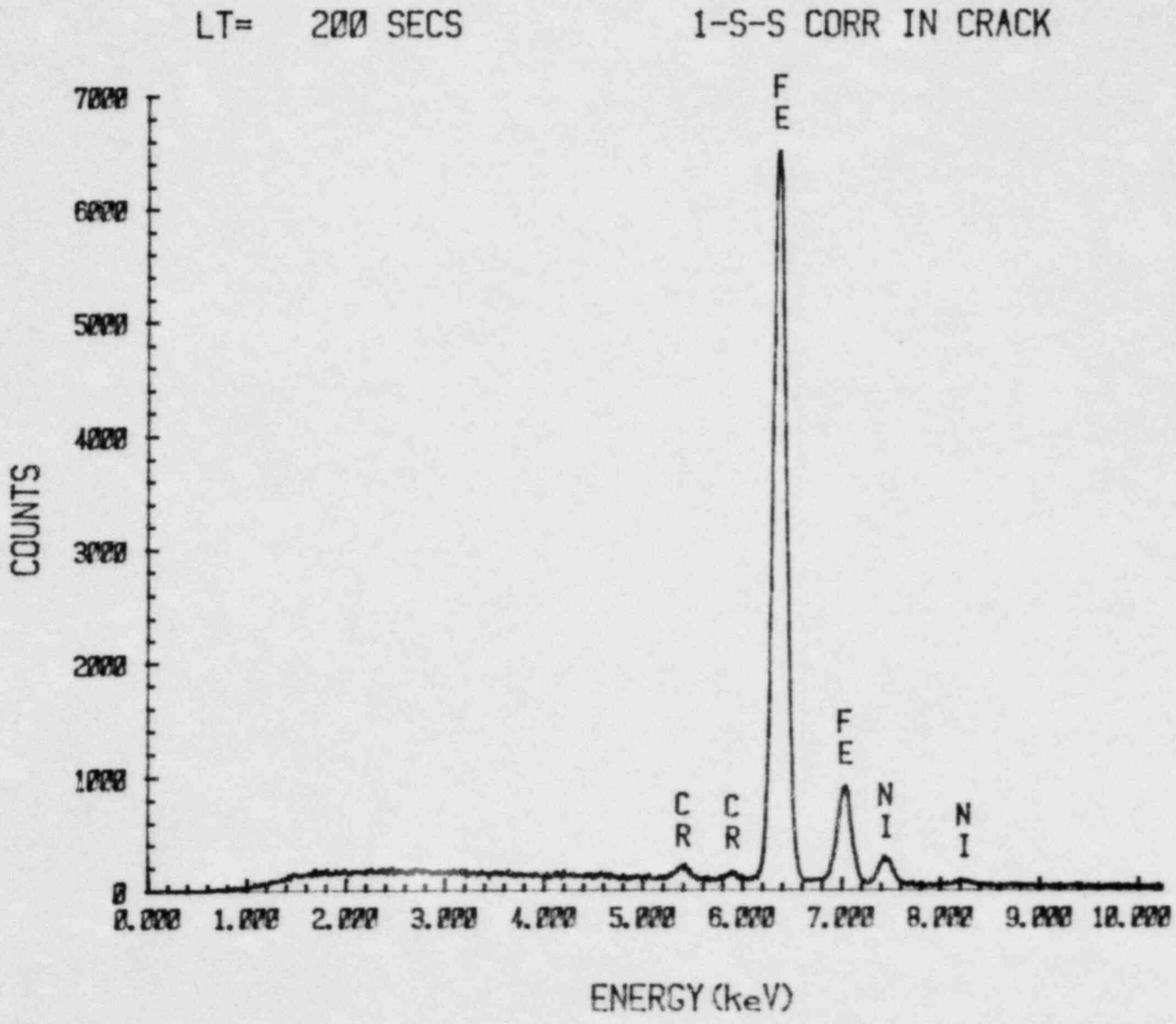

FIGURE 16. ENERGY-DISPERSIVE X-RAY SPECTRUM OBTAINED FROM AN ANALYSIS OF CORROSION PRODUCTS IN THE CRACK (AREA 4 IN TABLE 4)

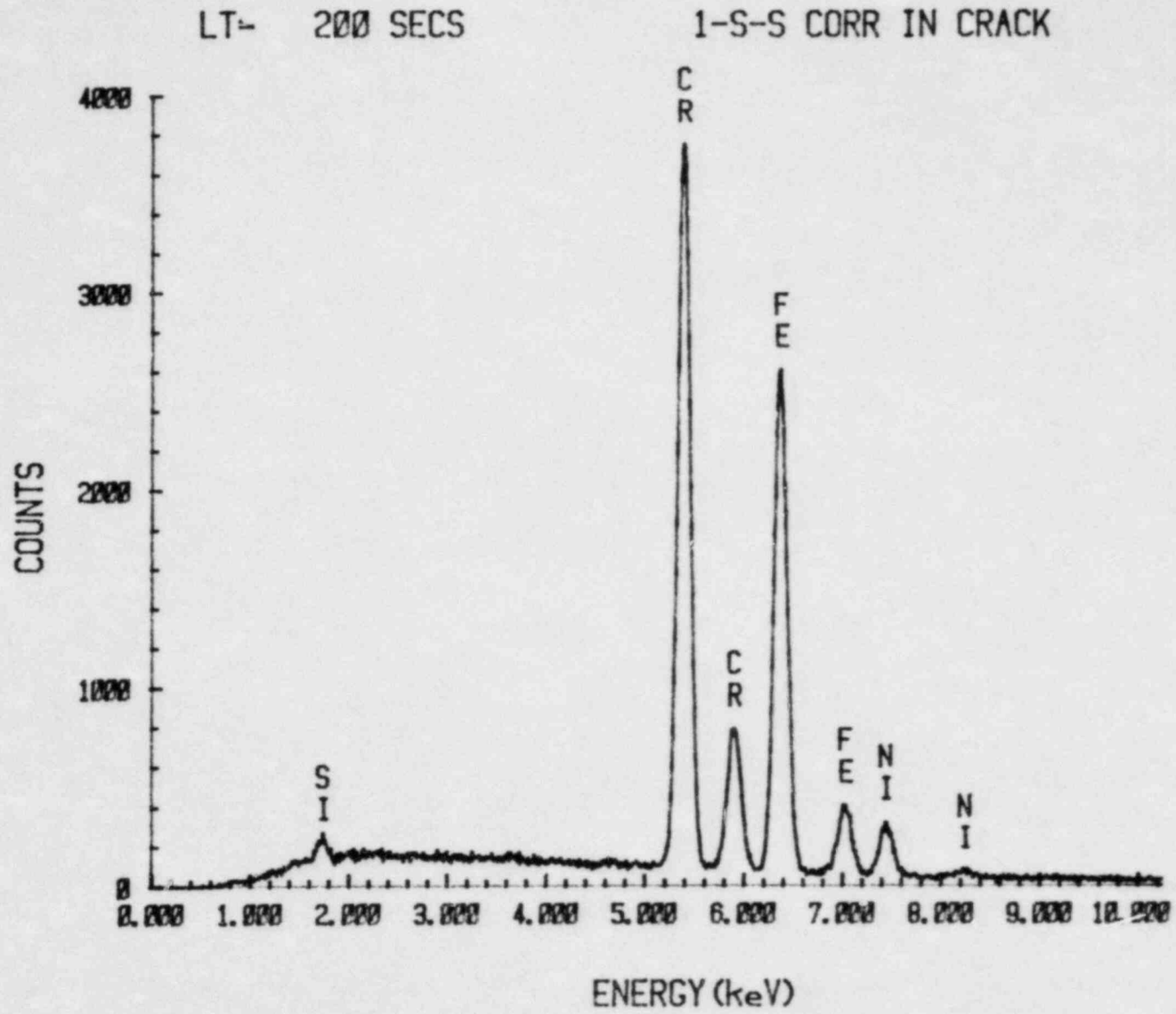

FIGURE 17. ENERGY-DISPERSIVE X-RAY SPECTRUM OBTAINED FROM AN ANALYSIS OF CORROSION PRODUCTS IN A BRANCH CRACK (AREA 6 IN TABLE 4)

chromium; the low chromium concentrations were similar to that found in the corrosion products in the main crack near the inside surface (Area 4 in Table 4).

A summary of the results presented in Table 4 indicates the following:

- The relative concentrations of nickel among the various corrosion products that were analyzed were on the order of 50 to 60 percent of the relative concentrations of nickel in the pipe or in the weld metal.
- The relative concentration of chromium in the corrosion products found along the principal IGSCC was significantly lower and the relative concentration of iron was significantly higher than those respective relative concentrations found in the pipe and in the weld metal.
- The relative concentrations of chromium and iron varied among the corrosion products in different branch cracks.
- The relative concentrations of iron, chromium, and nickel in the corrosion products in the surface flaw appeared to be similar to the concentrations of those elements in the corrosion products in branch cracks.
- The analyses of the pipe and the weld metal were similar, and they were nominally the same as the emission-spectrographic analyses obtained for those materials.

Corrosion Products in Flaw No. 2

The results of the EDAX electron-microprobe analyses of corrosion products observed within Flaw No. 2 are presented in Table 5. Those results were obtained from Specimen 2-N-N and Specimen 2-R-R of Flaw No. 2 (Specimen 2-N-N and Specimen 2-R-R of Flaw No. 2 are shown in Figures 9 and 10, respectively.)

Area 1 in Table 5 was located in the vicinity of the midlength of Flaw No. 2 with reference to Figure 9. The EDAX analysis of Area 1 was

TABLE 5. RESULTS OF SEMIQUANTITATIVE[a] ELECTRON-MICROPROBE ANALYSES OF CORROSION PRODUCTS BY ENERGY-DISPERSIVE-X-RAY ANALYTICAL TECHNIQUES IN SPECIMENS 2-N-N AND 2-R-R OF FLAW NO. 2

	Area Analyzed	Relative Concentration of the Elements Detected[b], percent						
		Fe	Cr	Ni	Si	Al	Ti	S
Specimen 2-N-N (Figure 9)								
1	Midlength of the flaw (see Figure 19a)	67.1	19.6	8.5	0.8	2.5	0.7	0.8
2	Large particle in the center of Figure 19a	23.0	56.1	ND[c]	ND	15.8	5.2	ND
3	Another area near Area 1	68.4	5.8	18.8	0.6	0.6	ND	5.8
4	Tip of the flaw	72.1	14.7	10.5	1.8	0.6	ND	0.2
Specimen 2-R-R (Figure 10)								
5	Midlength of the flaw	66.4	21.6	9.2	1.0	1.8	ND	ND
6	Tip of the flaw	44.1	48.3	6.0	1.1	ND	ND	0.5

(a) The semiquantitative analysis is a standardless quantitative analysis of the X-ray-energy-spectra data that includes a full ZAF (atomic number, absorption, and fluorescence factors) matrix-correction calculation. The relative concentrations of the elements detected are normalized to obtain a sum of 1.0 (100 percent).

(b) Elements lighter than Atomic Number 11 (sodium) are not detected, so oxygen could not be determined.

(c) ND = not detected.

obtained by an area scan at a magnification of 2000X. The X-ray-energy spectrum for Area 1 is presented in Figure 18; Area 1 is revealed in Figure 19a. Area 2 in Table 5 was a spot analysis of the large particle within Area 1 that is visible in the center of Figure 19a. Nickel, silicon, and sulfur were not detected in the large particle, whereas those elements, in addition to iron, chromium, aluminum, and titanium, were detected within Area 1 (Figure 19a) that included the particle. X-ray-distribution maps of the elements detected in Area 1, except silicon, are presented in Figures 19b through 19g. Figures 19f and 19g show, respectively, that the nickel and sulfur were concentrated in a small particle, apparently nickel sulfide, adjacent to the large particle.

The results presented in Table 5 seem to indicate that the composition of the corrosion products in Flaw No. 2 varies extensively from one area to another. The elements usually detected in the different areas were iron, chromium, nickel, aluminum, and silicon. Less frequently detected elements were titanium and sulfur.

Corrosion Products in Flaw No. 5

The results of the EDAX electron-microprobe analyses of corrosion products observed within Flaw No. 5 are presented in Table 6. Those results were obtained from Specimen 5-U-U (Figure 11) of Flaw No. 5.

The principal elements detected in the corrosion products in Flaw No. 5 were the same as those elements detected in the corrosion products in Flaw No. 1 and Flaw No. 2. As with those other flaws, variations in the compositions of the corrosion products were evident among different areas that were analyzed.

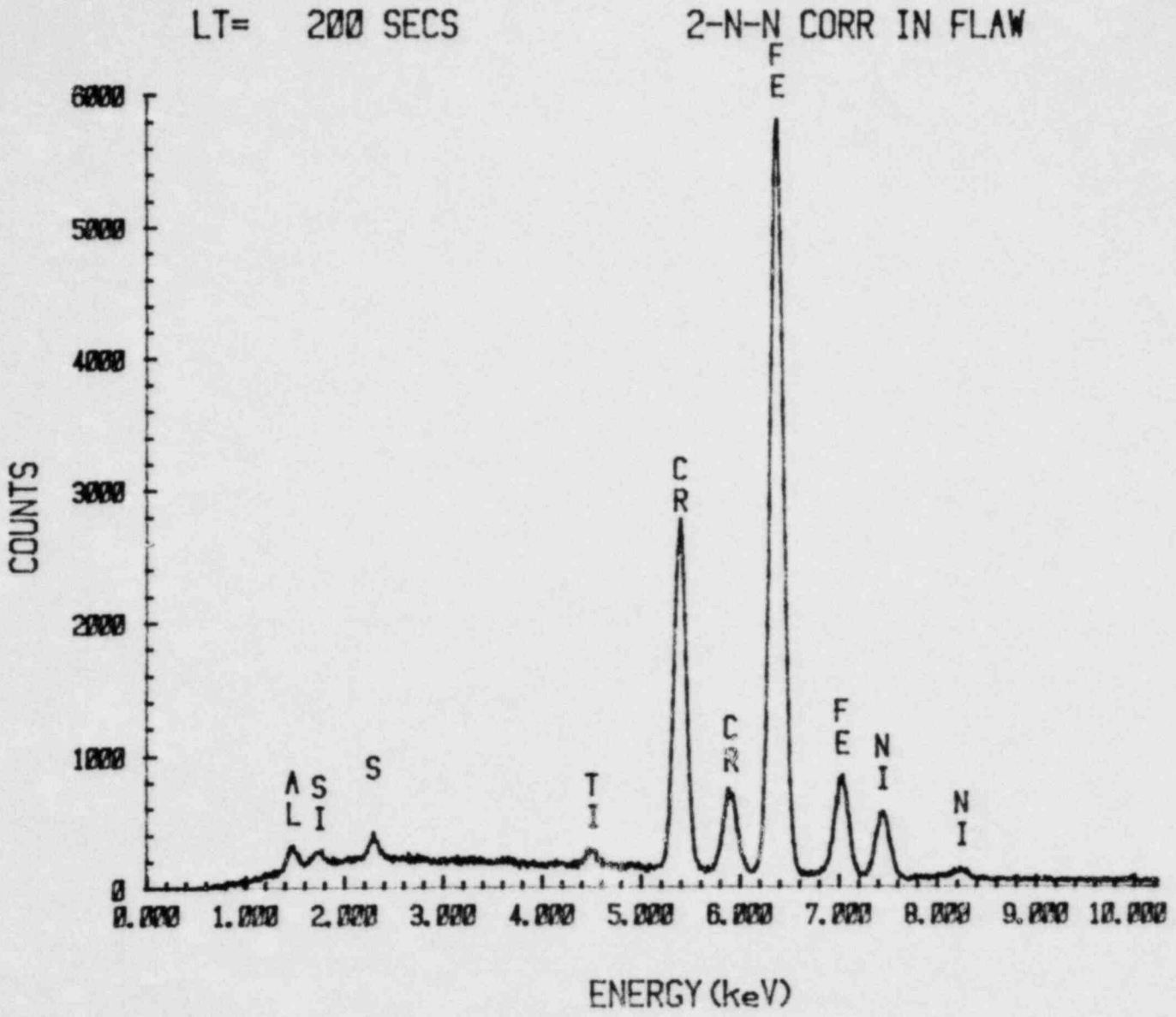

FIGURE 18. ENERGY-DISPERSIVE X-RAY SPECTRUM OBTAINED FROM AN AREA SCAN OF CORROSION PRODUCTS IN FLAW NO. 2, SPECIMEN 2-N-N (AREA 1 IN TABLE 5)

2000X 34696

a. Area 1 Reported in Table 5 (SEM Micrograph)

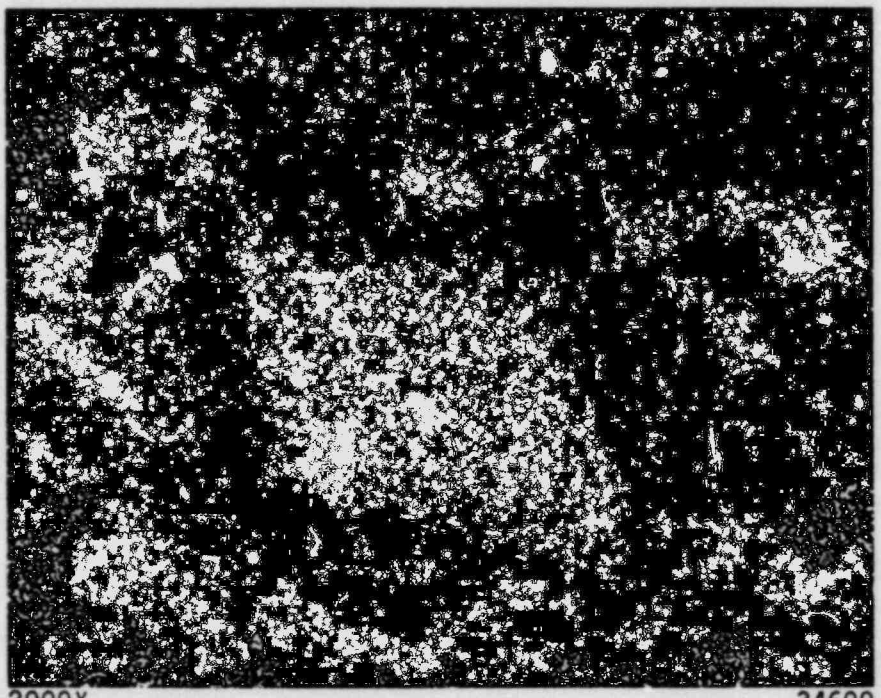

2000X 34699

b. X-ray-Distribution Map for Chromium in (a) Above

FIGURE 19. CORROSION PRODUCTS IN FLAW NO. 2 THAT WERE SUBJECTED TO ELECTRON-MICROPROBE ANALYSES

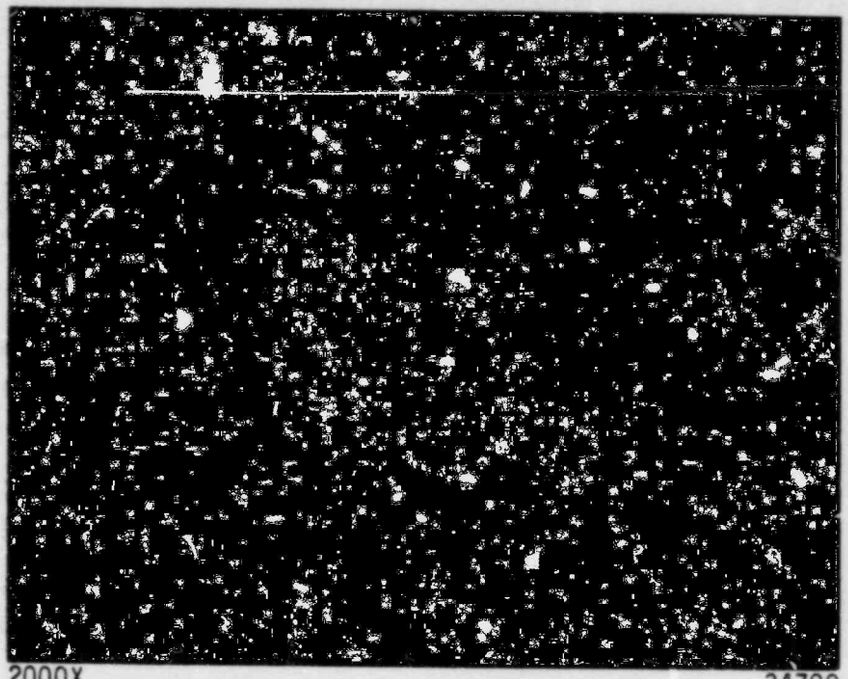

2000X 34700

c. X-ray-Distribution Map for Aluminum in (a) Above

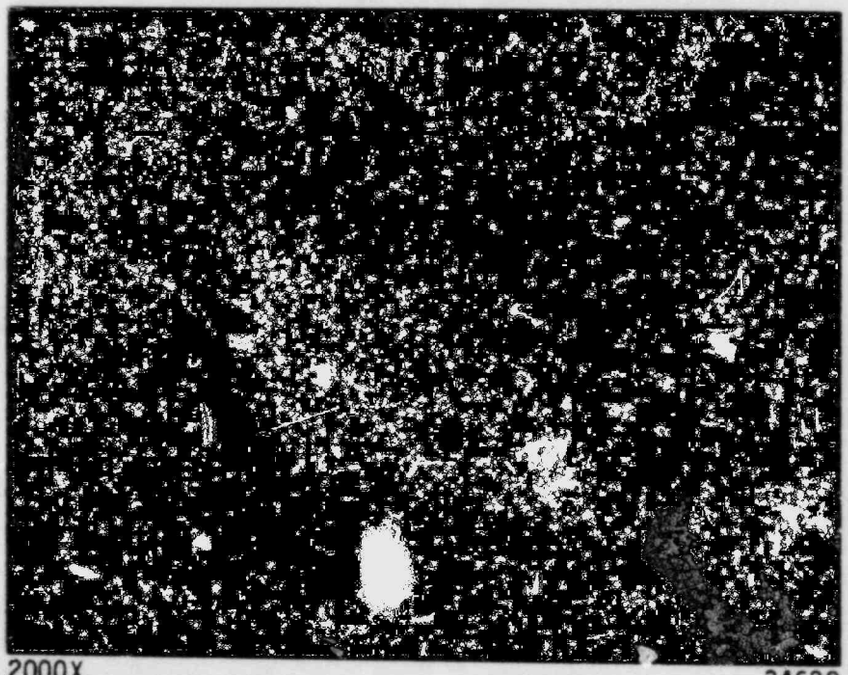

2000X 34698

d. X-ray-Distribution Map for Titanium in (a) Above

FIGURE 19. (Continued)

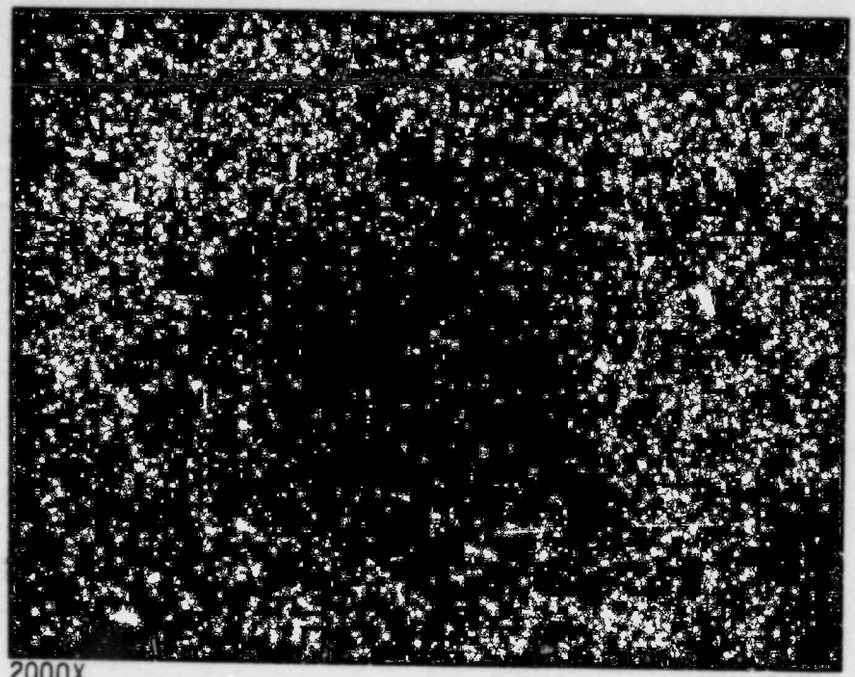

2000X 34702

e. X-ray-Distribution Map for Iron in (a) Above

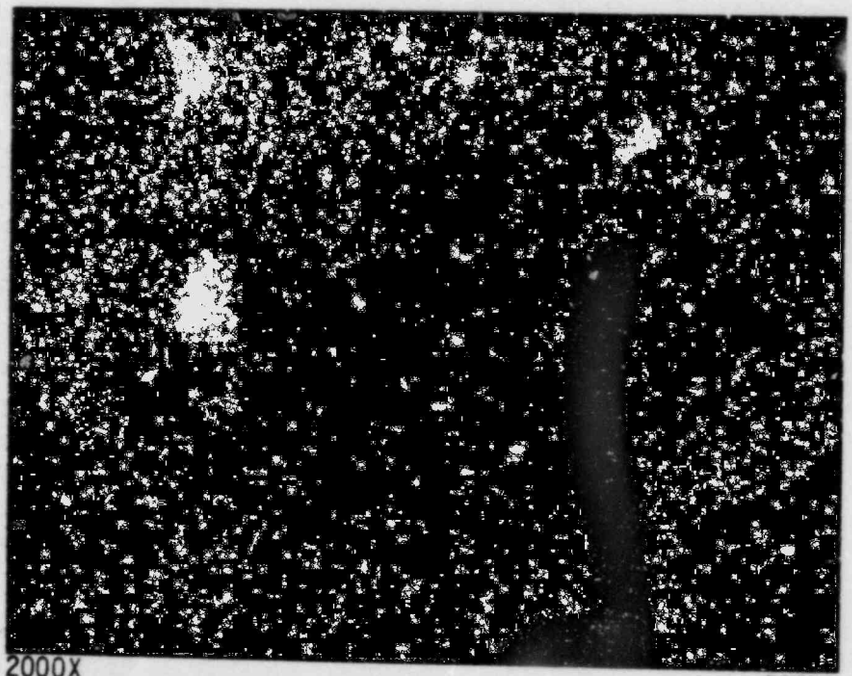

2000X 34701

f. X-ray-Distribution Map for Nickel in (a) Above

FIGURE 19. (Continued)

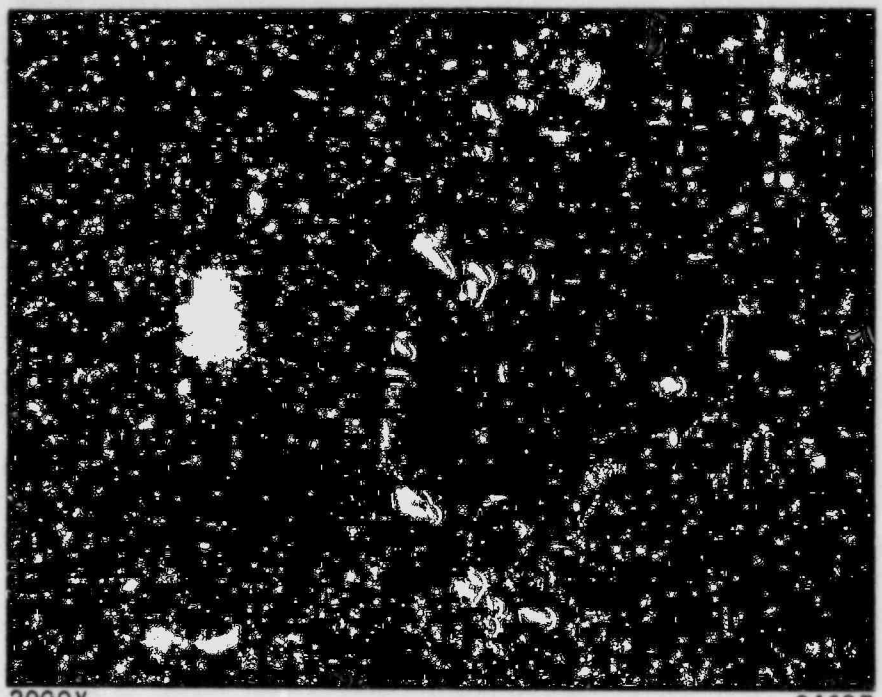

2000X 34697

g. X-ray-Distribution Map for Sulfur in (a) Above

FIGURE 19. (Continued)

TABLE 6. RESULTS OF SEMIQUANTITATIVE[a] ELECTRON-MICROPROBE ANALYSES OF CORROSION PRODUCTS BY ENERGY-DISPERSIVE X-RAY ANALYTICAL TECHNIQUES IN SPECIMEN 5-U-U OF FLAW NO. 5

	Area Analyzed	Relative Concentration of the Elements Detected[b], percent					
		Fe	Cr	Ni	Si	Al	S
1	Midlength of the flaw (see Figure 11)	86.9	2.3	9.1	1.5	ND[c]	0.3
2	Tip of the flaw	92.1	2.7	3.6	1.1	0.3	0.2

(a) The semiquantitative analysis is a standardless quantitative analysis of the X-ray-energy-spectra data that includes a full ZAF (atomic number, absorption, and fluorescence factors) matrix-correction calculation. The relative concentrations of the elements detected are normalized to obtain a sum of 1.0 (100 percent).

(b) Elements lighter than Atomic Number 11 (sodium) are not detected, so oxygen could not be determined.

(c) ND = not detected.

Electrochemical-Polarization-Reactivation (EPR) Tests

The EPR test* was developed by General Electric Company as a means to reveal the susceptibility of austenitic stainless steel piping to intergranular stress-corrosion cracking (IGSCC) in nuclear applications. The need for such a test arose from major problems in the past in the nuclear power industry with IGSCC in the weld-heat-affected zones of Type 304 stainless steel primary-coolant piping. The corrodent has been high-purity water that contained less than 9 ppm oxygen and less than 0.3 ppm chloride.

* Clarke, W. L., et al, "Detection of Sensitization in Stainless Steel Using Electrochemical Techniques", Paper 180, in Corrosion '77, National Association of Corrosion Engineers, Houston, Texas (1977).

Cihal, V., "A Potentiokinetic Reactivation Method for Predicting the I.G.C. and I.G.S.C.C. Sensitivity of Stainless Steels and Alloys". Corrosion Science, 20, 737 (1980).

In the EPR test, a stainless steel specimen, in a strong acid electrolyte, is cathodically cleaned and then held at an anodic potential to passivate the surface. The potential is then shifted in the cathodic direction through the corrosive range to test the passivating film produced previously. The resulting corrosion current during this shift (electrochemical reverse scan) is indicative of the degree of protection provided by the prior passivation treatment. A protective film will yield only a very small corrosion current, whereas a poorly protective film, such as the film over the chromium-depleted region adjacent to grain-boundary chromium carbides in a sensitized stainless steel, will yield a large corrosion current in the reverse scan. The ratio of the maximum corrosion current during the cathodic scan to the maximum corrosion current during the original anodic scan (EPR ratio) is used as a measure of the degree of sensitization. Limited experience has indicated that austenitic stainless steels having corrosion-current ratios of less than 0.04 in the EPR test are not sensitized and are not susceptible to intergranular cracking. Moreover, past experience with cast AISI 316 stainless steel indicated that material with an EPR ratio of approximately 0.01 was not susceptible to IGSCC, whereas material with EPR ratios that exceeded about 0.08 were susceptible. At the present time, a definite threshold value of the EPR ratio for the occurrence of IGSCC cannot be defined and probably varies with material.

The EPR tests were conducted during this investigation as a means of evaluating the degree of sensitization in the weld heat-affected zone and at the inside and outside surfaces of the subject pipe away from weld-heat effects. The initial EPR tests were made using an electrolyte that consisted of 2M H_2SO_4 and 0.1M KCL. Those tests showed no evidence of sensitization in either the weld-heat-affected-zone sample, EPR-2 in Figure 1, or the pipe samples, EPR-1 ID and EPR-1 OD, remote from the welded region. A review of the literature indicated that the electrolyte was probably too weak. The EPR tests were repeated, therefore, in an electrolyte that consisted of 2M H_2SO_4 and 0.5M KCl.

The results of the tests performed in the stronger solution are revealed in Figures 20 and 21 by a plot of current, mA, versus saturated

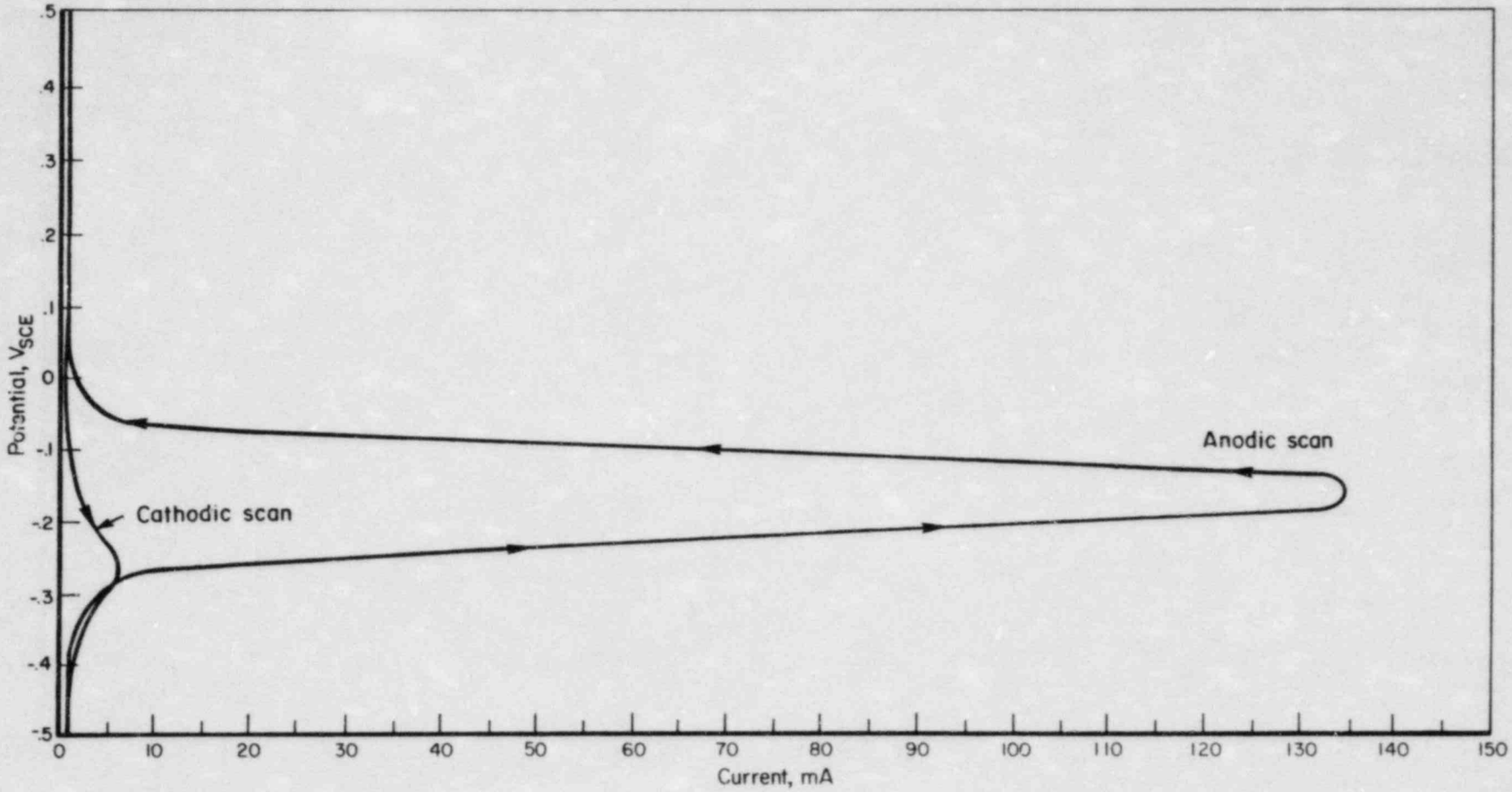

FIGURE 20. EPR CURVES FOR SAMPLE EPR-2 FROM THE WELD HEAT-AFFECTED ZONE

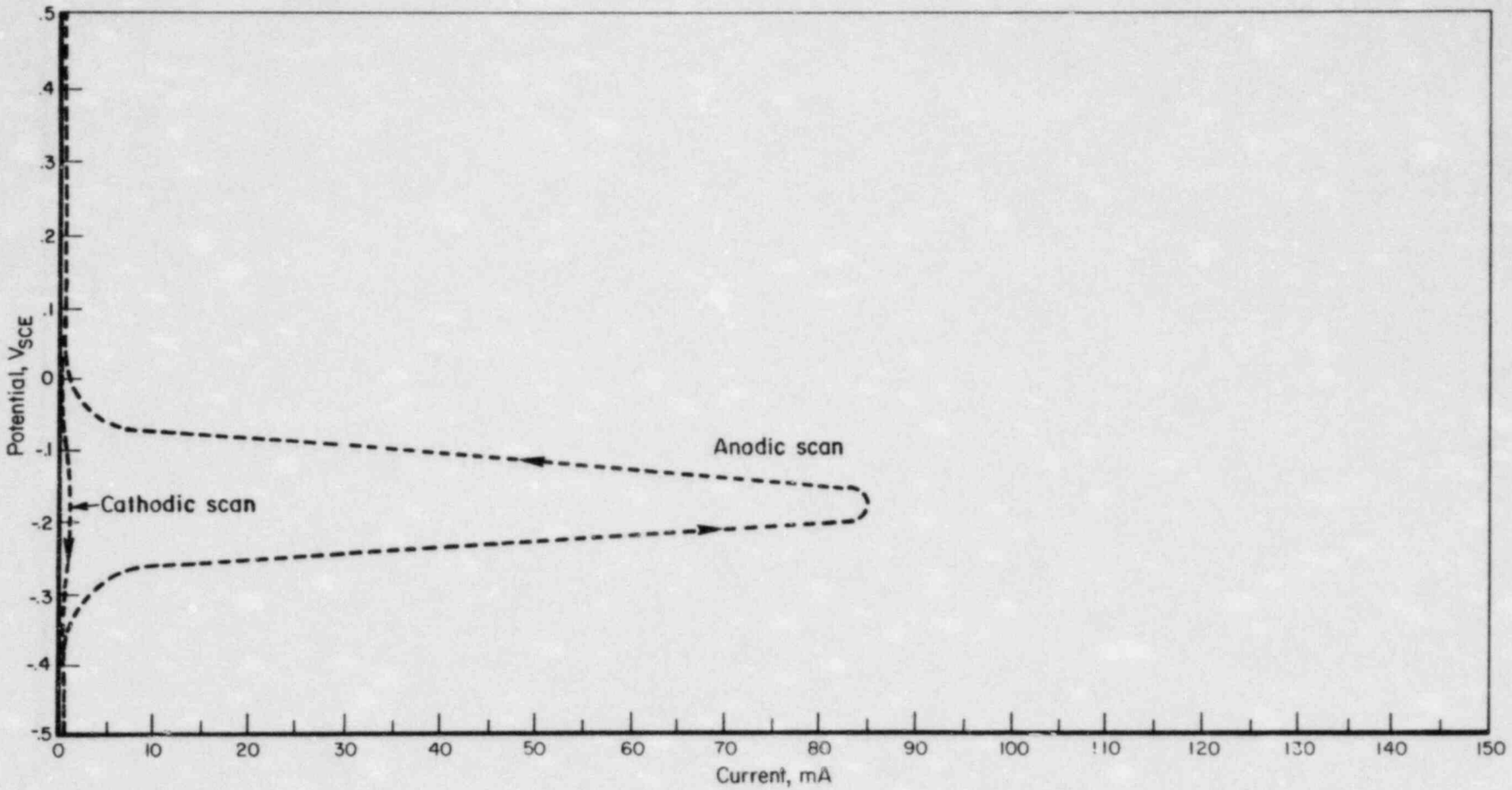

FIGURE 21. EPR CURVES FOR SAMPLES EPR-1 ID AND EPR-1 OD, AISI 304 STAINLESS STEEL PIPE REMOTE FROM THE REGION OF THE WELD

The same curve was obtained for both samples.

calomel electrode potential, V_{SCE}. For the weld heat-affected zone, the ratio of the maximum corrosion current during the cathodic scan to the maximum corrosion current during the original anodic scan was calculated to be 0.048 (Figure 20); the EPR ratio for the pipe samples remote from the welded region was calculated to be 0.009 (Figure 21). Thus, the weld heat-affected zone adjacent to the weld was more susceptible to IGSCC than was the stainless steel pipe. The higher susceptibility to IGSCC of the heat-affected zone apparently was a result of the sensitized condition of that zone.

DISCUSSION

The investigation of surface flaws revealed evidence similar to that reported in the earlier metallographic examinations, namely, evidence that the surface flaws were introduced during the production of the seamless pipe. The evidence indicated further that the fabrication-induced flaws were similar to laps or seams. Such flaws probably originated during the piercing operation.

IGSCC's were found to be associated with flaws that were located in the region of the girth-weld heat-affected zone; IGSCC's were not observed at flaws located outside the heat-affected zone. Metallographic examination revealed that the weld heat-affected zone had been sensitized. Based on the results of the EPR tests, the presence of IGSCC's in the weld heat-affected zone is not unexpected. The sensitized condition of the weld heat-affected zone apparently caused the zone to possess a degree of susceptibility to IGSCC, as was indicated by the EPR-test results; in the parent metal outside the heat-affected zone, no degree of susceptibility of the pipe to IGSCC was indicated. However, evidence of IGSCC was not observed in regions of the heat-affected zone where surface flaws were absent. Thus the presence of a surface flaw in the region of the heat-affected zone was apparently a major factor that contributed to the initiation of IGSCC. The contribution of the surface flaw to the onset of IGSCC was most likely in the manner of a stress raiser.

The profiles of the IGSCC's indicated that the major portions of the IGSCC surfaces were within the sensitized region underneath the surface flaws. The extremities of the cracks extended short distances beyond the ends of the flaws that were observed on the inside surface of the pipe. The depth of one crack below the inside pipe surface extended nearly through the thickness of the pipe wall and the other crack apparently penetrated the wall. For the most part, the propagation of the cracks appeared to be arrested in the through-wall direction by the broad, final passes of weld metal on the outside pipe surface and, in the pipe-axis direction, by the welded zone through the pipe wall at one end of the crack, and by the non-sensitized parent metal at the other end of the crack.

The electron-microprobe analyses of corrosion products in the surface flaws and in the IGSCC's did not identify the presence of a specific corrodent. Most likely the corrodent was the water in the core-spray system that contained low concentrations of oxygen and perhaps chloride that could not be detected by energy-dispersive X-ray analysis.

CONCLUSIONS

The results of the investigation led to the following conclusions:

- Linear indications on the inside pipe surface were fabrication-induced surface flaws.
- IGSCC was associated only with surface flaws that were located in the region of a sensitized weld heat-affected zone.
- Surface flaws acting as stress raisers were a major factor that led to the initiation of IGSCC.
- In the weld heat-affected zone, the IGSCC's extended through most of the pipe wall.
- Propagation of IGSCC was apparently arrested by weld metal and nonsensitized parent metal that surrounded the weld heat-affected zone.
- In the absence of the fabrication-induced surface flaws, IGSCC may not have occurred in the weld heat-affected zone.

ATTACHMENT